Svalbard surface snowpack Azzurra Spagnesi^{a,b}, Elena Barbaro^{a,b} *, Matteo Feltracco^{a,b}, Federico Scoto^{c,b}, Marco Vecchiato^b, Massimiliano Vardè^a, Mauro Mazzola^a, François Burgay^{d,e}, Federica Bruschi^f, Clara Jule Marie Hoppe^g, Allison Bailey^g, Andrea Gambaro^{a,b}, Carlo Barbante^{a,b}, Andrea Spolaor^{a,b} ^a Institute of Polar Sciences - National Research Council of Italy (ISP-CNR), Via Torino 155, 30172, Venice, Italy ^b Department of Environmental Sciences, Informatics and Statistics, Ca' Foscari University of Venice, Via Torino 155, 30172, Venice, Italy ^c Institute of Atmospheric Sciences and Climate - National Research Council of Italy (ISAC-CNR), Campus Ecotekne, Lecce, 73100, Italy ^d Laboratory of Environmental Chemistry (LUC), Paul Scherrer Institut (PSI), Villigen, 5232, Switzerland ^e Oeschger Centre for Climate Change Research, University of Bern, Bern, 3012, Switzerland f Department of Chemistry, Biology and Biotechnology, University of Perugia, Via dell'Elce di Sotto 8, 06123, Perugia, ^g Alfred Wegener Institute, Helmholtz Centre for Polar and Marine Research, 27570 Bremerhaven, Germany Corresponding: Elena Barbaro (elena.barbaro@cnr.it)

Seasonal and interannual variability on the chemical composition of the

Abstract

Arctic Amplification (AA) is driving long-term changes in the Arctic climate system, including glacier ice melt, rapid sea ice decline, and alterations in atmospheric and geochemical processes, with consequences on the formation, transport, and chemical composition of aerosols and seasonal snowpack. Svalbard, particularly vulnerable to AA, provides a valuable site to assess changes in local environmental processes contributing to the seasonal snow chemical composition. From 2018 to 2021, sampling campaigns at the Gruvebadet Snow Research Site in Ny-Ålesund, in the North-West of the Svalbard Archipelago, captured the interannual variability in ionic and elemental impurities within surface snow, reflecting seasonal differences in atmospheric and oceanic conditions. Notably, warmer conditions prevailed in 2018-19 and 2020-21, contrasting with the relatively colder season of 2019-20. Our findings suggest that impurity concentrations in the 2019-20 colder season are impacted by enhanced sea spray aerosol production, likely driven by a larger extent of sea ice, and drier, windy conditions. This phenomenon was particularly evident in March 2020, when extensive sea ice was present in Kongsfjorden and around Spitsbergen due to an exceptionally strong, cold stratospheric polar vortex and unusual Arctic Oscillation (AO) index positive phase. By comparing the snow chemical composition of the 2019-20 season with 2018-19 and 2020-21, we provide insights into the interplay between short-term meteorological variability and the long-term climatic impacts of AA in Svalbard, as well as associated shifts in aerosol production process.

1. Introduction

Chemical analysis of surface Arctic snow and ice can provide valuable comprehension of the composition of Arctic aerosols, its deposition, and exchange processes (Lai et al., 2017). These processes are influenced by a range of factors, including Arctic Amplification (AA) – a pronounced, long-term increase in near-surface air temperature observed since 1975 (Chylek et al., 2022). AA is recognized as an inherent characteristic of the global climate system, with multiple intertwined causes operating on a spectrum of spatial and temporal scales. These include, but are not limited to, changes in sea ice extent that impact heat fluxes between the ocean and the atmosphere, and water vapor that alters longwave radiation (Serreze and Barry, 2011). The Svalbard Archipelago is particularly sensitive to these effects due to the relatively low altitude of its main ice fields and its geographical location in the higher North Atlantic, where the impact of AA is especially pronounced (Spolaor et al., 2024). Therefore, in the 21st century, predicting and characterizing climate change in Svalbard is particularly crucial, as changes in near-surface air temperature, precipitation, and sea ice extent occur at an extremely high pace (Gjermundsen et al., 2020; Rantanen et al., 2022). The Svalbard region,

located at the southern edge of the seasonal Arctic sea-ice zone, is characterized by a maritime climate 63 with strong temperature variations during winter (Hansen et al., 2014; Barbaro et al., 2021). In the 64 Arctic winter, the stratospheric polar jet fosters a high-atmospheric vorticity zone. This winter vortex 65 typically acts as a strong barrier for the long-range transport of pollutants from mid-latitudes 66 (Lawrence et al., 2020). However, it occasionally allows warm southern air to penetrate the region 67 (Schoeberl and Newman, 2015). Additionally, Svalbard frequently experiences intense cyclonic 68 storms in autumn and winter, which bring both heat and moisture from lower latitudes (Rinke et al., 69 2017). These intense meteorological variations, generally linked with a weaker polar vortex (Sobota 70 71 et al., 2020; Salzano et al., 2023), favor long-range transport of aerosols to the archipelago, including pollutants from continental sources (Stohl et al., 2006b; Yttri et al., 2014a; Vecchiato et al., 2024; 72 73 D'Amico et al., 2024).

Arctic snow captures dry and wet deposition and forms an archive that includes a range of seasonal 74 chemical species such as major ions and trace elements, as well as human-made pollutants emitted 75 into the Arctic atmosphere (Koziol et al., 2021). Ny-Ålesund is a well-monitored area and a natural 76 77 laboratory for complex system observations, ideal for exploring both long-range contaminants from mid- to high-latitude regions of Eurasia and Canada (Nawrot et al., 2016; Song et al., 2020; Vecchiato 78 79 et al., 2024; D'Amico et al., 2024), and local inputs from both natural processes and human settlement 80 (Vecchiato et al., 2018). Previous research has extensively investigated the chemistry of Arctic snow and the exchange of inorganic species between the cryosphere and the atmosphere across multiple 81 82 sites, including Barrow, Summit Greenland, Alert, Sodankylä, and over the Arctic Ocean during the 83 MOSAiC expedition (e.g., Beine et al., 2003; Björkman et al., 2013; Jacobi et al., 2019). Specific studies in Ny-Ålesund and surrounding areas have explored the temporal and compositional aspects 84 85 of the lower atmosphere (Stohl et al., 2006a; Eleftheriadis et al., 2009; Geng et al., 2010; Zhan et al., 2014; Feltracco et al., 2020, 2021; Turetta et al., 2021), though relatively few have addressed the 86 87 detailed seasonal dynamics of snow-atmosphere interactions in this region. Building on this existing research, our study aims to enhance the understanding of these interactions, particularly in the context 88 89 of recent climatic changes.

In this study, we evaluate the surface snow concentration of ionic (Cl⁻, Br⁻, NO₃⁻, SO₄²⁻, MSA, Na⁺, 90 NH₄⁺, K⁺, Ca²⁺) and elemental impurities (Li, Be, Mg, Al, Ca, V, Cr, Mn, Fe, Co, Ni, Cu, Zn, As, Se, 91 Rb, Sr, Ag, Cd, Sb, Cs, Ba, Tl, Pb, Bi, U) for the snow seasons between 2018-2021, at the Gruvebadet 92 Snow Research Site (GSRS) location, 1 km south of Ny-Ålesund, where clean and undisturbed snow 93 conditions 94 are guaranteed throughout the whole sampling season. The differences in average meteorological and climatological conditions across the studied seasons 95

are analysed to assess how sea ice extent, polar vortex, and Arctic Oscillation (AO) conditions influence the composition of surface snow in connection with the aerosol-producing and deposition processes in Kongsfjorden. Additionally, a Kruskal-Wallis's test, followed by Dunn's post-hoc analysis, has been employed to identify species most affected by inter-annual and seasonal variations, with the goal of uncovering potential correlations between meteorological-climatic conditions and chemical concentrations.

Three sampling campaigns were conducted in Svalbard between 2018 and 2021, covering the period

2. Methodology

96

97

98

99

100

101

102

103

104

2.1 Sampling and processing

105 from October to May according to the onset of the snowpack formation and melting. Sample collection followed the protocol presented in Spolaor et al. (2019), further adopted by Bertò et al. 106 107 (2021), where consecutive and adjacent sampling was carried in a 3x3 meters snow sampling area, 108 within a clean sampling snowfield of 100 m wide. Each sample was collected 10 cm apart from the previous one, along a precise path. This method was designed to minimise the temporal variability 109 between consecutive samples and reduce the impact of potential spatial variability (within the 5-15%) 110 range, according to Spolaor et al., 2019). 111 During the first sampling campaign, carried out from October 4th, 2018 to May 10th, 2019, 114 surface 112 snow samples were collected in a delimited snow field located ~ 100 m south of the "Dirigibile Italia" 113 Station" in Ny-Ålesund (78.92° N 11.93° E, Ny-Ålesund, Svalbard). The surface snow was sampled 114 within the upper 3 cm, as this is the snow layer most impacted by aerosol deposition and exchange 115 processes at the snow-atmosphere interface (Spolaor et al., 2018, 2021b). This choice also minimised 116 the effect of different physical snow conditions (density, crystal shape, and size). 117 Concurrently, additional 133 snow samples were collected at the Gruvebadet Snow Research Site 118 (GSRS) to evaluate the spatial variability with respect to the snow samples collected in Ny-Ålesund. 119 The GSRS is a clean-area located about 1 km south of Ny-Ålesund, nearby the Gruvebadet 120 Atmospheric Laboratory (GAL), dedicated to the chemical and physical monitoring of the seasonal 121 snowpack (Scoto et al., 2023; Fig. 1). Throughout the season, the sampling resolution varied based 122 on light conditions. During the polar night (from October to early March), snow sampling was carried 123 out daily at Ny-Ålesund, and every 3-5 days at the GSRS. With the beginning of the polar day, daily 124 sampling was conducted both in Ny-Ålesund and at the GSRS in March, and then continued only at 125 126 the GSRS until the end of the snow season in June due to the lower contamination of the site, more 127 distant from the fervent local activities. This sampling resolution overlap during March ensured a good comparison of results in both snow fields (Fig. S1). 128

- Starting from the second campaign, snow sampling activities were conducted only at the GSRS site,
- since clean conditions of the field in Ny-Ålesund could not be guaranteed due to construction works.
- The snow sampling was carried out from October 26th, 2019 to May 25th, 2020, with a total of 107
- samples collected. The surface snow layer was sampled every 3-5 days during the polar night (until
- February 24th, 2020), and daily from the beginning of the polar day until the end of the snow season.
- 134 Consecutive samples represent the same snow layer in the absence of snowfall or wind drift/erosion.
- However, factors such as snow aging, potential element re-emission, transformation, and dry
- deposition can introduce variability, making continuous monitoring essential.
- Finally, during the third snow sampling campaign, lasting from October 27th, 2020 to June 15th, 2021,
- a weekly sampling was conducted at GSRS, with a total of 32 samples collected.
- During snow sampling, the temperature and density of surface snow were measured, and the density
- of snow was calculated based on weighting a 100 cc cylinder. After collection, snow samples were
- melted, and two different aliquots were obtained and stored in separate vials. In a 1.5 mL
- polypropylene (PP) vial, 1 mL of sample was stored for ionic species, while another aliquot was
- stored in a 5 mL LDPE vials for trace elements analysis. PP vials designated to ionic species analysis
- were previously sonicated for 30 min in UltraPure Water (UPW) (18 MΩ cm⁻¹ at 25 °C) for
- decontamination. LDPE vial used for trace elements analysis were instead conditioned with HNO₃
- 2% and sonicated for 30 min. All sample aliquots were stored at -20°C in dark conditions and
- transported to the Venice ISP-CNR laboratories.
- 148 To assess potential contamination during sampling, handling, and transport, field blanks were
- 149 collected during each campaign. Metal-free vials (Avantor, VWR Centrifuge Tubes, CHN) were
- opened to ambient air at the sampling sites for a few minutes without collecting snow, then sealed
- and transported to the Ny-Ålesund laboratory. There, they were filled with 2% HNO₃ and stored under
- the same conditions as the snow samples. In parallel, analytical blanks were prepared by opening
- vials to air, sealing them, and transporting them directly to Venice, where they were filled with 2%
- 154 HNO₃ and ultrapure water from the laboratory. Both field and analytical blanks were analyzed
- alongside the snow samples, confirming that background contamination levels were below detection
- limits for all target analytes.
- Furthermore, seawater temperatures and salinity at 10 m depth were also monitored in Kongsfjorden
- 158 (Kb3; 78°57.228'N, 11°57.192'E) during 2019-2021 spring seasons, with data collected every 3-6
- days (Assmy et al. 2023). Data was derived from Conductivity Temperature Depth (CTD) casts with
- either a MiniSTD model SD-204 (SAIV A/S, Bergen, Norway) or a XR-620 CTD (RBR Ltd, Ottawa,
- 161 Canada). Combined casts of both instruments conducted in May 2020 and 2021 did not reveal
- differences in temperature or salinity in the reported accuracy (two post comma digits).

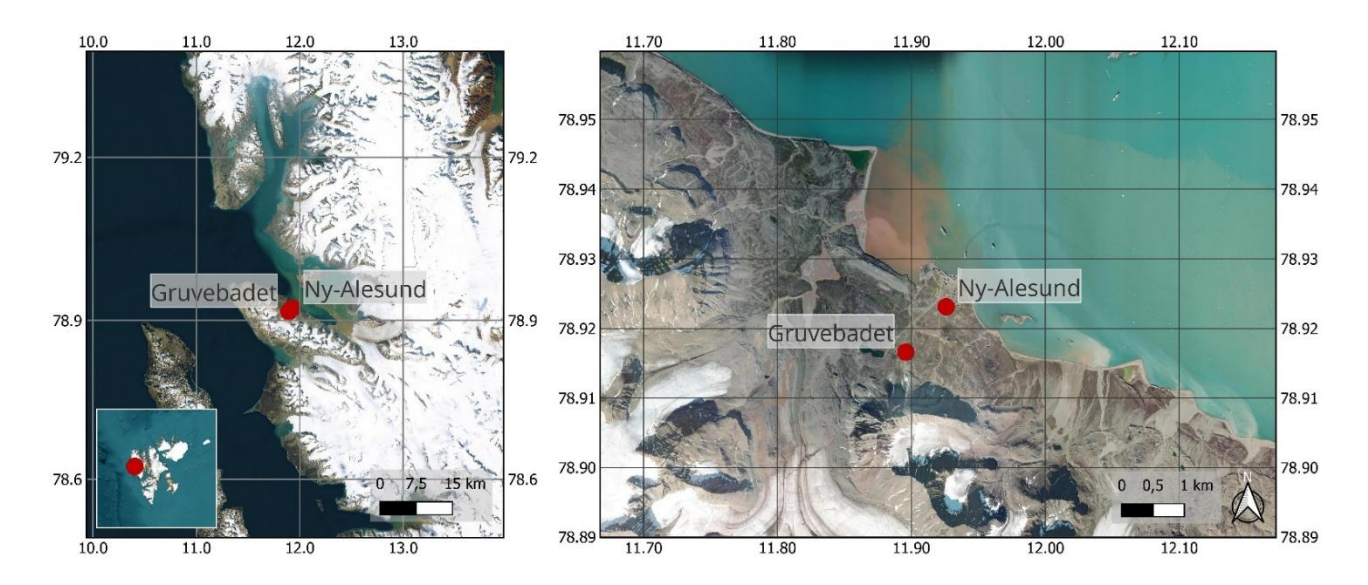


Fig. 1. Sampling sites of Ny-Ålesund and Gruvebadet, located in the Brøgger peninsula (Svalbard Islands).

2.2 Analysis of ionic species

163

164

165

166

167

168

169

170

171

172

173

174

175

176

177

178

179

180

181

182

183

184

185

The analysis of anionic species (Cl⁻, Br⁻, NO₃⁻, SO₄²-, MSA) was carried out using an ion chromatograph (IC, Thermo Scientific Dionex™ ICS-5000, Waltham, MA, USA) coupled with a single quadrupole mass spectrometer (MS, MSQ PlusTM, Thermo Scientific, Bremen, Germany). The separation was performed using an anionic exchange column (Dionex Ion Pac AS 19 2 mm ID × 250 mm length) equipped with a guard column (Dionex Ion Pac AG19 2 mm ID × 50 mm length). Sodium hydroxide (NaOH), used as mobile phase, was produced by an eluent generator (Dionex ICS 5000EG, Thermo Scientific). The NaOH gradient with a 0.25 mL min⁻¹ flow rate was: 0-6 min at 15 mM; 6-15 min gradient from 15 to 45 mM; 15-23 min column cleaning with 45 mM; 23-33 min equilibration at 15 mM. The injection volume was 100 µL. A suppressor (ASRS 500, 2 mm, Thermo Scientific) removed NaOH before entering the MS source. The IC-MS operated with a negative electrospray source (ESI) with a temperature of 500°C and a needle voltage of 3 kV. The other MS parameters are reported by Barbaro et al. (2017). The same IC system was simultaneously used to determine cationic species (Na⁺, K⁺, Ca²⁺ and NH₄⁺). However, Ca²⁺ was not measured within the samples collected during the second campaign due to instrumental limitations. The separation occurred with a capillary cation-exchange column (Dionex Ion Pac CS19-4 mm 0.4 mm ID × 250 mm length), equipped with a guard column (Dionex Ion Pac CG19–4, 0.4 mm ID × 50 mm length), and the species were determined using a conductivity detector. Analytical blanks of ultrapure water (> 18 M Ω cm) were included in the analysis, and the Method Detection Limit (MDL) was set to 3 times the standard deviation of the blank values. Checks for accuracy were made using certified multi-element standard solutions for anions (Cl., Br., NO₃-, SO₄²-, no. 89886-50ML-F, Sigma

- Aldrich) and cations (Na⁺, K⁺, Ca²⁺, no. 89316-50ML-F, Sigma Aldrich) at a concentration of 10 mg
- 187 $L^{-1} \pm 0.2\%$. The analytical precision was quantified as the relative standard deviation (RSD) for
- replicates (n > 3) of standard solutions and was always < 10% for each ion.
- 189 *2.3 Trace Elements analysis*
- 190 Twenty-six elements (Li, Be, Mg, Al, Ca, V, Cr, Mn, Fe, Co, Ni, Cu, Zn, As, Se, Rb, Sr, Ag, Cd, Sb,
- 191 Cs, Ba, Tl, Pb, Bi and U) were analyzed on samples previously melted and acidified to 2% v/v with
- 192 HNO₃ (UpA grade, Romil, UK) for 24 hours before analysis (Spolaor et al., 2018; Spolaor et al.,
- 193 2021a).
- The analysis was performed using Inductively Coupled Plasma Mass Spectrometry (ICP-MS, iCAP)
- 195 RQ, Thermo Scientific, US). The ICP-MS was equipped with an ASX-560 autosampler (Teledyne
- 196 Cetac Technologies), PolyPro PFE nebulizer, PFE cyclonic spray chamber thermostated at 2.7°C,
- sapphire injector, quartz torch and Ni cones. The acquisition was performed at 1550 W of plasma RF
- power in Kinetic Energy Discrimination (KED) high matrix mode, using He as collision gas (4.3
- mL min⁻¹). Instrument parameters were optimized for best sensitivity in the whole mass range,
- 200 minimum oxides (< 1%) and double charges (< 3%). Quantification was obtained by external
- calibration with multi-elemental standards prepared in ultrapure water (18 M Ω cm⁻¹ at 25° C) with
- 202 2% v/v ultrapure grade HNO₃ (UpA grade, Romil, UK), with a combination of certified level multi-
- elemental solutions IMS-102 and IMS-104 from UltraScientific. Analytical quality control was
- performed by memory test blank (repeated analysis of ultrapure grade HNO₃ 2% v/v blank solution)
- after each sample and calibration verification (repeated analysis of reference standards) every 11
- samples. More details are found in Spolaor et al., 2021a.

207208

2.4 Transport modelling, sea ice, Kongsfjorden condition, and polar vortex

- The Lagrangian particle dispersion model HYSPLIT (Draxler, 1998; Stein et al., 2015) was used to
- determine the source region of air masses over Ny-Ålesund. This model has previously been shown
- 212 to be an effective tool for the prediction of transport pathways into and within the Arctic and Antarctic
- 213 regions (Barbaro et al., 2015; Feltracco et al., 2021). The simulations were driven using
- 214 meteorological data from the Global Data Assimilation System (GDAS) one-degree archive, set the
- 215 top of the model at 10000 m and the height source equal to the GSRS altitude. Back-trajectories were
- calculated every 6 h, with a propagation time of 120 h for each sampling period. The choice of a 6-
- 217 hour interval for the calculation of back-trajectories allows for the capture of temporal variability in
- 218 air mass origins over the day, which is particularly important in polar regions where atmospheric

circulation patterns can change rapidly. This temporal resolution strikes a balance between computational efficiency and the need for sufficient detail to characterise the variability in source regions during each sampling period. The propagation time of 120 hours was selected to provide an adequate temporal window to trace long-range transport pathways that influence air mass composition at Ny-Ålesund. This configuration is consistent with previous studies on atmospheric circulation in the same site (Feltracco et al., 2021).

This approach was used to ensure an envelope working for all investigated tracers. The resulting multiple trajectories were based on the screen-plot analyses of total spatial variance.

The Ice Service provided by the Norwegian Meteorological Institute (NIS) was employed to analyse the weather conditions via remotely sensed data and to generate ice charts of Svalbard, ice-edge information, and sea surface temperatures trends. Sea ice extent variability in Kongsfjorden was evaluated based on dataset made available by Gerland et al. (2022).

Differences between the sampling campaigns were evaluated through the National Centers for Environmental Prediction/National Center for Atmospheric Research (NCEP/NCAR) Reanalysis data from NOAA Physical Sciences Lab's daily composites tool, used to calculate the near-surface air temperatures across the Northern Hemisphere from October to May.

Results below the limit of detection were assumed to be equal to ½ of Method Determination Limit

(MDL) prior to perform statistical analysis, to approximate their likely level based on the data

2.5 Statistical procedures and Enrichment Factors (EFs) Analysis

distribution curve (best approximated as log-normal for most of the studied variables) (George et al., 2021). The Wilcoxon rank-sum test was applied on data from the 2018–19 sampling campaign to assess whether there was a statistically significant difference in the surface snow contamination levels (ionic loads) between the two sites: Ny-Ålesund and Gruvebadet. This model assumes that the data is sampled from two matched or dependent populations, and data is assumed to be continuous. Because it is a nonparametric test, it does not require a particular probability distribution of the dependent variable in the analysis. Furthermore, Enrichment Factors (EFs) using Ba as a crustal element of reference (Widepohl, 1995; Spolaor et al., 2021a; Ruppel et al., 2023), were calculated to explore the mixed sources of the investigated elements. To complement the EFs analysis, a Hierarchical Cluster Analysis (HCA) was performed using Ward's algorithm and Euclidean distances as clustering criteria, to determine the presence of some clusters and simplify the interpretation of the dataset.

Additionally, to examine the inter-annual and seasonal variations in chemical's concentrations and to identify the species most affected by these changes, a Kruskal-Wallis' test was employed, followed by Dunn's post-hoc test for pairwise comparisons. The Kruskal-Wallis' test, a nonparametric alternative to Anova, which is typically applied when samples do not follow a normal distribution (Van Hecke, 2013), was chosen to assess differences in chemical concentrations across the years of sampling campaigns and multiple seasons. This allowed for an objective evaluation of temporal differences in concentration levels, while Dunn's post-hoc analysis, which uses the same shared rankings and pooled variance assumed under the Kruskal-Wallis null hypothesis, helped identify which specific seasons showed statistically significant differences from each other. The Bonferroni correction was used for the Dunn's test to control for false positives when performing multiple pairwise comparisons (Dunn, 1961).

The ultimate goal of this analysis was to uncover potential correlations between meteorologicalclimatic conditions and chemical concentrations in surface snow, helping to better understand how environmental factors contribute to contamination trends.

These combined statistical approaches provided a comprehensive framework for analysing the complex dataset.

3. Results

3.1 Comparison between concentration trends at Gruvebadet and Ny-Ålesund

The concentration variations between an undisturbed area in Ny-Ålesund village and GSRS sites were compared during the 2018-19 sampling campaign to better understand the effect of spatial variability between the two sampling sites. The concentration trends of Na⁺, as sea salt tracer, Pb as anthropogenic species, and Ca²⁺ as crustal tracer, are reported in Fig. S1, for both sampling sites. Although the difference in time resolution between sites is apparent in Fig. S1, the difference in concentration trends appears not statistically significative (p values < 0.05, Wilcoxon test) for all the analysed species, except for sporadic peaks in sea salt and crustal tracers present in the Ny-Ålesund record from November to February. These peaks do not consistently correlate with positive temperature anomalies and precipitation events, as some occurred under low temperatures and without significant precipitation (e.g., January and early February), suggesting that other processes, such as long-range transport, wind-driven deposition, or dry deposition may also play a role (Fig. S1). Concordant Pb trends emerge at Ny-Ålesund and Gruvebadet, with the highest concentrations observed from February to May.

To evaluate the differences in concentration range and spatial distribution of surface snow impurity content, we applied the Wilcoxon test for the 2018-19 sampling period by comparing the distributions for positive and negative differences of the ranks of their absolute values. This comparison is crucial for assessing spatial variability in the measured parameters, providing context and serving as a reference for local-scale differences. However, at a significance level of 0.01, the two distributions from GSRS and Ny-Ålesund sites appeared not statistically different for all the trace elements and most of the inspected ions, except for Na⁺, K⁺, NO₃⁻, Br⁻, and MSA – which are typical sea salt and biological species (MSA).

For this reason, only the GSRS temporal trend has been considered throughout the manuscript, referring to ionic loads (mg m $^{-2}$) instead of concentrations (ng g $^{-1}$), to highlight the seasonal trends of specific tracers. The ionic load is calculated as ionic concentrations multiplied by the density and the thickness of sampled strata.

3.2 Interannual trends of chemical species on the surface snow

Three consecutive snow seasons were evaluated to define the chemical composition of the surface snow in the Arctic site of GSRS. The sea salt ions Cl⁻ (50 %), and Na⁺ (23%) represent the most abundant species, followed by SO₄²⁻ (11 %), Mg (7 %), Ca (2%), Fe (1%) and Al (1%). Similar relative concentration abundances were also found in previous studies on the snow of the Svalbard Archipelago (Beaudon and Moore, 2009; Vega et al., 2015; Barbaro et al., 2021; Spolaor et al., 2021b).

Table 1 reports the average ionic loads of the most abundant (> 1%) species in the surface snow, considering three different seasons: autumn is defined until December 21st, winter until March 21st, and spring from then to the melt onset, identified by 5-6 consecutive days of negative snow accumulation. The average ionic loads of the less abundant (< 1%) species are reported instead in Table S1.

Table 1. Average ionic loads of the most abundant (>1%) ionic and elemental species in the surface snow during each season of the three consecutive sampling campaigns. The standard deviation is shown in brackets, while in the case of nss- SO_4^{2-} the brackets represent the percentage of nss- SO_4^{2-} compared to the total SO_4^{2-} . "n" indicates the number of samples considered for the calculation of the average.

mg m ⁻²	Total	Cl	Na ⁺	SO ₄ ² -	nss-SO ₄ ²⁻	Mg	Fe	Ca	NO ₃ -	K ⁺	NH ₄ ⁺
autumn 2018 (n=22)	32	15	7	3	1	3	2	0.3	0.5	0.3	0.04
	(25)	(21)	(11)	(4)	(36%)	(3)	(5)	(0.3)	(0.5)	(0.4)	(0.03)
winter 2018-19 (n=41)	116	55	31	16	8	8	0.4	0.4	2	2	0.3
	(80)	(68)	(39)	(16)	(51%)	(8)	(0.3)	(0.3)	(2)	(2)	(0.3)
spring 2019 (n=51)	76	36	19	9	4	6	2	0.6	1	1	0.5
	(50)	(43)	(24)	(9)	(48%)	(5)	(3)	(0.4)	(1)	(1)	(0.4)
autumn 2019 (n=15)	214	101	40	26	16	10	1	9	5	2	4
	(98)	(71)	(53)	(20)	(61%)	(6)	(1)	(12)	(4)	(3)	(5)
winter 2019-20 (n=43)	339	159	79	41	21	16	2	9	3	3	7
	(120)	(88)	(73)	(20)	(52%)	(8)	(5)	(10)	(2)	(4)	(8)
spring 2020 (n=49)	273	110	52	28	15	21	6	13	4	2	5
	(132)	(91)	(77)	(25)	(53%)	(21)	(9)	(16)	(2)	(4)	(8)
autumn 2020 (n=6)	803	435	191	66	18	84	1	2	6	9	2
	(542)	(466)	(205)	(83)	(27%)	(165)	(2)	(5)	(11)	(10)	(2)
winter 2020-21 (n=13)	327	207	64	41	24	6	0.2	0.2	5	3	1
	(203)	(194)	(48)	(36)	(60%)	(5)	(0.4)	(0.1)	(3)	(2)	(1)
spring 2021 (n=13)	181	107	36	16	7	9	4	1	3	2	1
	(92)	(86)	(26)	(12)	(43%)	(10)	(7)	(2)	(2)	(2)	(1)

The average loads of the first sampling year were lower compared to the other campaigns (Fig. S2; Table 1).

High average loads were observed instead for Cl⁻ and Na⁺ in the top snowpack layer during the 2019-20 and 2020-21 winter seasons. The highest concentrations of sea salt species were found in autumn 2020, despite low snow accumulation (17.25 cm) in a period of relatively high precipitation (4.91 mm) (Fig. 2, Table S3). This apparent contradiction can likely be attributed to the increased wind speeds during that time, which may have caused snow redistribution, thereby limiting accumulation despite the considerable precipitation.

The non-sea-salt sulphate (nss-SO₄²⁻), calculated using a seawater SO₄²⁻/Na⁺ mass ratio of 0.252 (Millero et al., 2008), was the most abundant fraction of the total sulphate in autumn 2019 and winter 2020-21, while in autumn 2018 and 2020 sea salt sulphate (ss-SO₄²⁻) was the dominant fraction. No clear predominance between the two fractions was achieved during the other investigated seasons, which may reflect a more mixed influence of marine and continental sources (Table 1).

The abundance of all chemical species investigated is quite similar for all years (Fig. S2), although the sampling campaign 2019-20 showed higher percentage of calcium ranging between 3% and 5%, in contrast to the typical concentrations < 1% found in the other two campaigns.

To further examine differences in species concentrations across seasons and years, a Kruskal-Wallis test was performed. The test indicates significant differences ($\chi^2 > 15.51$, df = 8, p-value = 0.05) for

several species across the nine seasons of the three sampling campaigns. These species include Br

341 $(\chi^2 = 16.9)$, MSA $(\chi^2 = 81.3)$, SO₄²⁻ $(\chi^2 = 21.3)$, nss-SO₄²⁻ $(\chi^2 = 23.4)$, Bi $(\chi^2 = 19.2)$, Cd $(\chi^2 = 31.9)$,

- 342 Cu ($\chi^2 = 44.5$), Fe ($\chi^2 = 21.9$), Pb ($\chi^2 = 45.1$), Ni ($\chi^2 = 20.6$), Ag ($\chi^2 = 24.5$), U ($\chi^2 = 22.1$), V ($\chi^2 = 22.1$)
- 343 40.9), Zn ($\chi^2 = 29.9$). To identify which seasons accounted for these differences, a Dunn's test with
- Bonferroni correction was applied as a post-hoc test, revealing significant seasonal differences for
- multiple elements (Fig. S3), with pronounced differences particularly between autumn and winter,
- and between spring and winter (P.adj \leq 0.05; Table S5).
- Finally, correlations between meteo-climatic variables (air temperature, wind speed, wind direction,
- precipitation, AO index) and the concentrations of the selected species were computed to assess
- potential meteorological influences. The results indicated generally weak positive correlations (ρ <
- 350 0.5) for the variables considered. Notably, MSA showed a correlation with air temperature ($\rho = 0.2$),
- as did Bi ($\rho = 0.2$), Cu ($\rho = 0.2$), Fe ($\rho = 0.2$), Pb (0.1), Ni, ($\rho = 0.2$), Ag ($\rho = 0.2$), U ($\rho = 0.3$), V ($\rho = 0.3$
- 352 = 0.3), and Zn (ρ = 0.3).

353

354

355

356

357

358

359

360

361

362

363

364

365

366

367

368

369

370

371

372

3.3 Polar vortex and Arctic Sea ice extent in 2019-20

According to the 2023 survey conducted by the National Snow and Ice Data Center (NSIDC), the maximum extent of Arctic Sea ice since 2014 has been recorded in March 2020, with 14.73 million square kilometres of the Arctic Ocean surface, in a decadal trend characterized by a -2.53% of decline, due to the Arctic Amplification. Considering the Kongsfjorden area, the total sea ice extent varied from 63.94 km² in March 2019 to 129.81 km² in March 2020, and was with 46.26 km² lowest in March 2021 (Gerland et al., 2022). Specifications on Drift Ice (DI), Fast Ice (FI), and Open Water (OW) extent are reported in Table S2. The 2020 maximum sea ice extent followed the exceptionally strong and cold stratospheric polar vortex that took place in the Northern Hemisphere (NH) during the 2019-20 polar winter, together with low wave activity from the troposphere, which allowed the polar vortex to remain relatively undisturbed (Lawrence et al., 2020). Notably, the 2020 Arctic Sea ice extent is 16% and 9% higher than previous (2018-19) and following (2020-21) records (dataset NSIDC, NOAA). Lower surface mean air temperatures (-14.7°C, compared to the -11.4°C recorded in 2018-19, and the -8.0°C recorded in the 2020-21), average reduced precipitations (2.1 mm compared to 2.6 mm in 2018-19, and 3.2 mm in 2020-21), higher maximum mean wind speed (17.7 ms⁻¹ for 6 days, compared to 15.4 ms⁻¹ for 3 days in 2018-19, and 13.8 ms⁻¹ for 5 days in 2020-21), and higher mean snow height (62.63 cm compared to 58.06 cm in 2018-19, and 57.77 cm in 2020-21) were observed during the 2019-20 winter season, attributed to the influence of a strong polar vortex triggered by a net positive Artic Oscillation (AO) phase. The 2020 anomalous AO index is displayed in Fig. S4. Seasonal values of mean air temperatures (°C), mean precipitation (mm), maximum mean wind speed (m sec⁻¹) and mean snow depth (cm) during the three consecutive sampling campaigns are reported in Table S3. Temperature data were provided by the Norwegian Centre for Climate Services (NCCS), while sea ice extent data were supplied by National Snow and Ice Data Center (NSIDC). Seawater temperature data collected at 10 m depth at a mid-fjord station near Ny-Ålesund (Kb3) was found to be colder during 2020 compared to 2019 and 2021 spring seasons (Table S4). Although these temperatures were still above the freezing point for the observed salinity levels, they contributed to colder overall conditions in Kongsfjorden, supporting the formation and prolonged presence of sea ice when combined with cold atmospheric conditions.

4. Discussion

4.1 Ny-Ålesund seasonal and interannual trends variability in surface snow

The three consecutive sampling campaigns conducted from 2018 to 2021 confirmed the dominance of sea salt input in the surface snow of Svalbard, due to the proximity of the sampling sites to the coastline (Barbaro et al., 2021). The dominant ions are Na⁺, Cl⁻, and SO₄²⁻, associated with the scavenging precipitation of marine aerosol (Hodgkins and Tranter, 1998). The observed mean seasonal trends (Fig. S2) display the highest concentrations of marine species in autumn 2020, followed by 2020-21 and 2019-20 winter seasons. However, wintry concentrations are presumably linked to weakened (2019-20) or destroyed (2020-21) polar vortex (Fig. 2) and intense cyclonic storms, associated with anomalous warming events capable of transporting both heat and moisture from lower latitudes to Svalbard (Rinke et al., 2017). In addition to these factors, it is important to account for snow ablation or erosion by wind. The change in snow height (Δh) between consecutive sampling events provides valuable insights into such processes. A decrease in snow height signals ablation can indeed result from snow melting (under positive temperatures), snow aging, sublimation, or snow drift. In particular, when wind speeds exceed 5 m s⁻¹, the threshold commonly accepted for initiating snow drift and ablation episodes (Pomeroy, 1989), we can infer the snow erosion due to wind drift likely occurred (Fig. 2). This effect may explain some of the variability in snow ion concentrations, especially during intense storms or strong winds.

Autumn 2020 represents most likely an outlier, due to scarce precipitations (Fig. 3) that led to more concentrated impurities in the surface snow. In contrast, late spring 2020 saw a notable increase in typical marine ions (Na⁺, Cl⁻, Br-, MSA, SO₄²⁻) and geogenic elements (Al, Ca, Mn, Fe, Sr), compared to spring 2019 (Fig. 3). This increase may be attributed to the very close drift Arctic Sea ice presence in Kongsfjorden (Table S2), which reached its maximum extent in March 2020 due to low-temperature anomalies and intensified atmospherically driven sea ice transport and deformation,

caused by higher than normal winter wind speeds (Fig. S5). These conditions likely enhanced the production of sea spray aerosols, which, when carried by winds, may have increased the deposition of marine species onto the snowpack. The increased deposition of geogenic elements might also have been influenced by low temperature anomalies (as seen with Fe), and/or by stronger wind speeds, although significant correlations have not emerged in this preliminary statistical analysis. Additionally, an outstanding positive phase of the Arctic Oscillation (AO) in the troposphere (Fig. 2) was recorded in January-March 2020 (Lawrence et al., 2020; Dethloff et al., 2022). Although the entire period was remarkable, January and February featured as clear outliers in the historical timeseries (1950–2023) reported by the NOAA service, while March 2020 exhibited significantly elevated values but did not exceed the statistical threshold for outliers (Fig. S4).

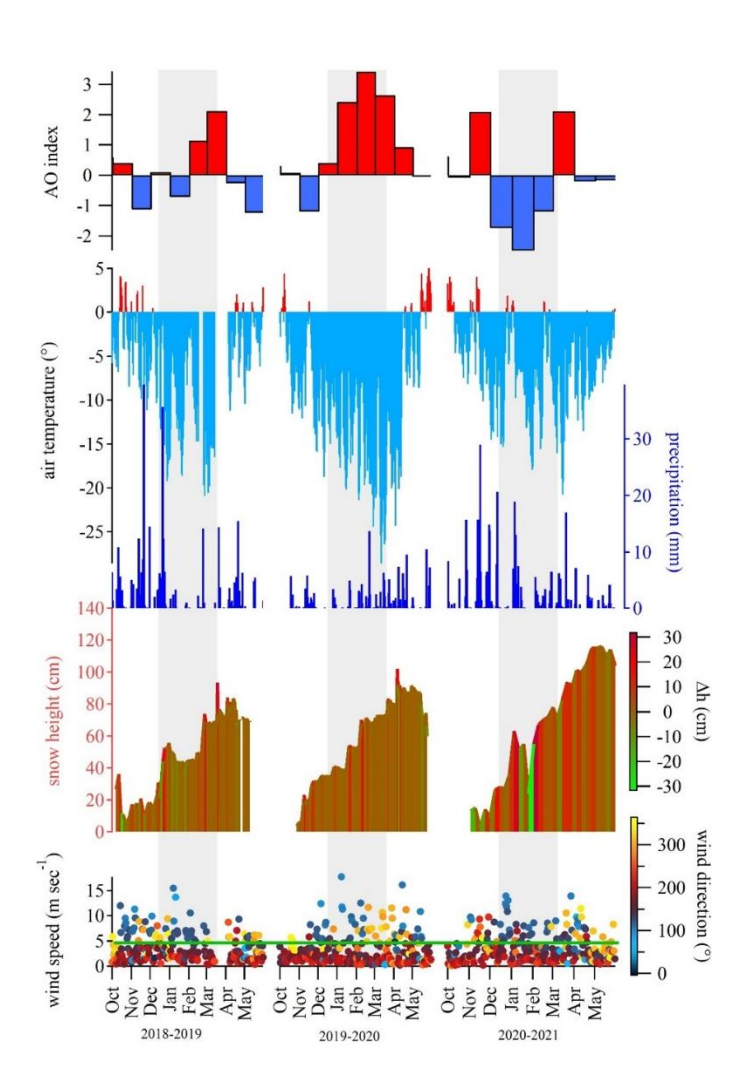


Fig. 2. AO Index, air temperature (°C), precipitation (mm), snow height (cm), Δh snow height (cm), wind speed (m sec⁻¹), and wind direction (°) from the NCEP/NCAR Reanalysis data. The green horizontal line above the wind speed graph indicates the 5 m sec⁻¹ threshold, above which wind drift may occur on surface snow layers. The colour of the line refers to the Δh color scale, which indicates negative values of Δh , NOAA Physical Sciences Lab's daily composites tool was used to calculate the near-surface air temperatures across the Northern Hemisphere from October to May. Grey bands indicate the winter periods.

A 2021 spring peak of marine species was also recorded, although more attenuated than in spring 2020 (Fig. 3, Fig. S2). This variation is likely attributable to different extents of sea ice in the fjord. Nonetheless, seawater temperatures in 2021, similar to those in 2020 and 2.3°C colder than in 2019 (Table S4), along with comparable wind speed conditions (Fig. S5), may also have contributed to the observed trends in marine species concentrations. Similarly, the spring peak of Mg, Sr, Mn, Fe, Al, and V in 2021 seems to reflect the high wind speed and positive AO index recorded from March to April 2021. Positive anomalies for air temperatures (A) and wind speed (W) conditions, together with negative anomalies in seawater (O) conditions were observed during the 2020-21 campaign, while negative A and O conditions were accompanied to positive W during 2019-20. On the contrary, 2018-19 diverges from the other campaigns for positive O condition associated to negative W condition anomalies. These observations provide valuable insights into how shifts in atmospheric and oceanic conditions impact the concentrations of ionic and elemental species in surface snow, enhancing our understanding of the underlying mechanisms that govern these changes in the context of AA conditions.

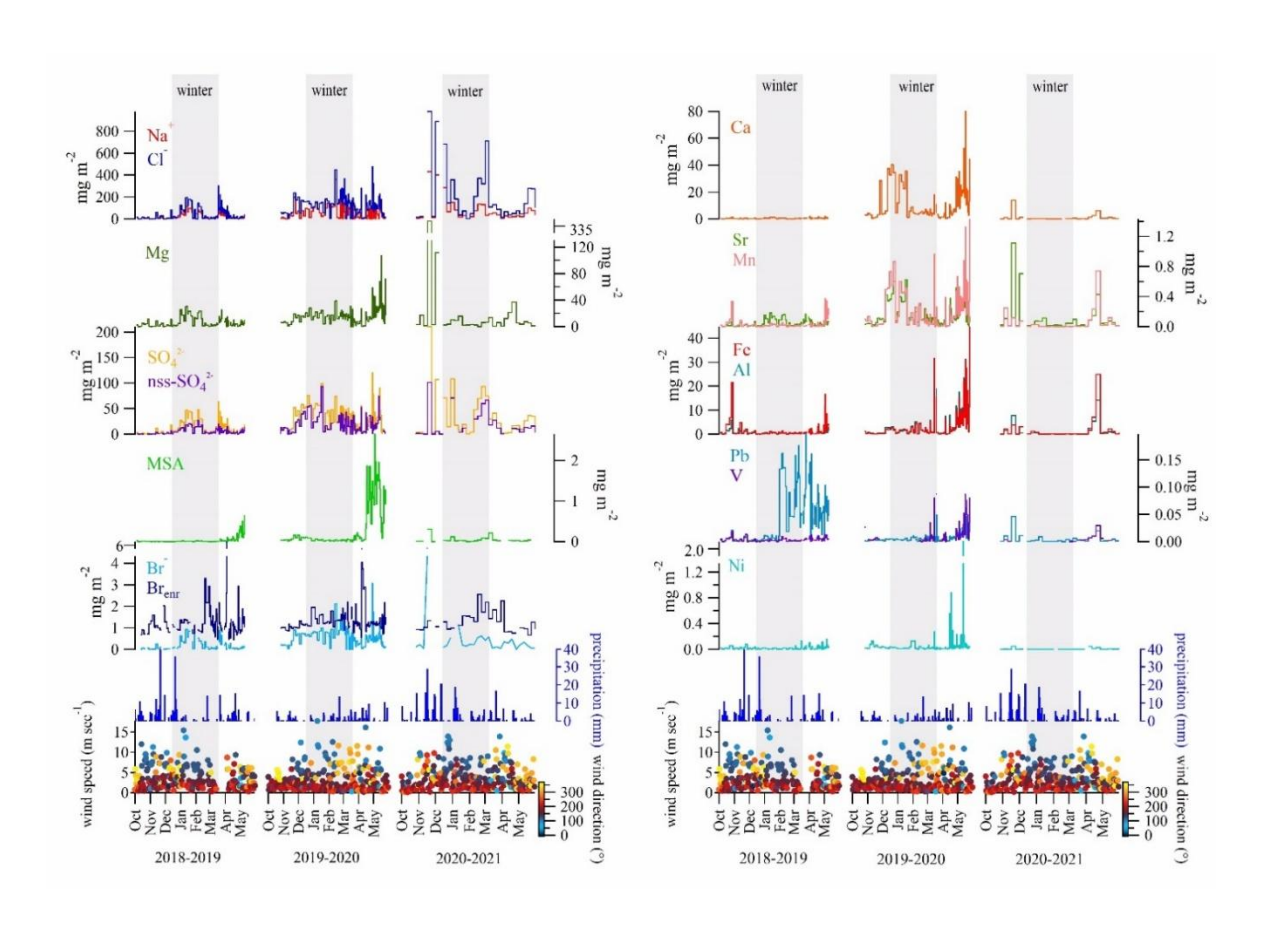


Fig. 3. Wind direction (°), wind speed (m sec⁻¹), and ionic loads (mg m⁻²) of Na⁺, Cl⁻, Mg, SO₄²⁻, nss-SO₄²⁻, MSA, Br⁻, Ca, Sr, Mn, Fe, Al, Pb, V, Ni in the surface snow for the three sampling campaigns: 2018-19, 2019-20, 2020-21. Seasonal trends are here presented for specific elements to provide a detailed view of how concentrations vary across distinct sampling periods.

A singular case is represented by Pb, which showed a 12.5-fold increase during winter-spring 2019 period compared to autumn 2018. The EF for Pb during these seasons exceeded 100, indicating a strong anthropogenic contribution. In contrast, the peak observed in 2020 no longer shows such elevated EF values (i.e., EF = 26), suggesting a mixed source (Fig. 4). This implies that the April-May 2020 peak is largely of crustal origin, as the overlap with V (EF < 10) also suggests, possibly due to local dust events driven by strong winds exceeding the 5 m sec⁻¹ threshold (Fig. 3; Table S3).

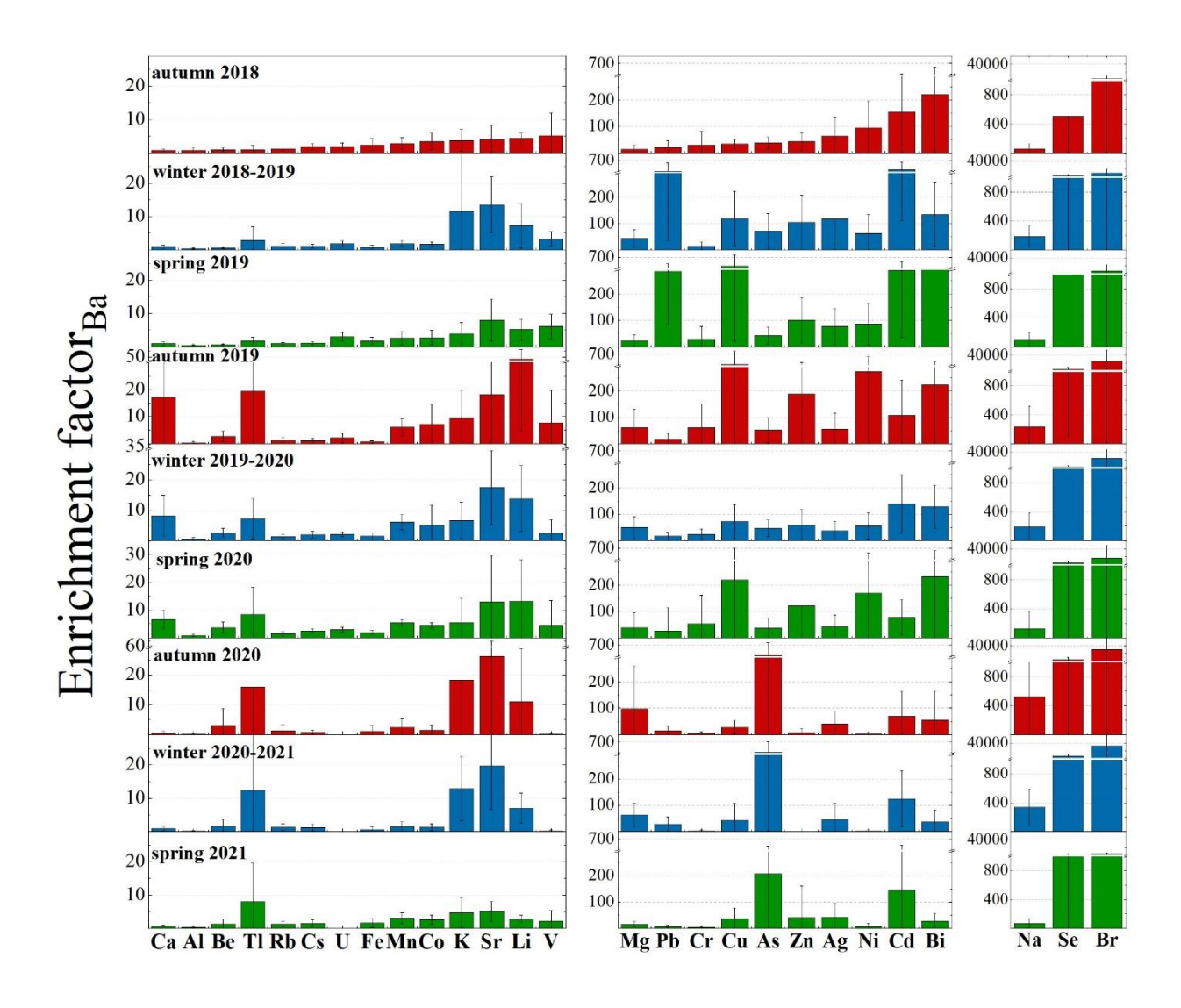


Fig. 4. Enrichment Factors (EFs) calculated on all the presented trace elements for the three sampling campaigns: 2018-19, 2019-20, 2020-21. Calculating EFs for the full dataset offers a more robust assessment of potential sources and enrichment patterns, minimizing the variability inherent in individual seasons and allowing for a clearer distinction between crustal and non-crustal contributions.

The calculated EFs (Fig. 4) for Be, Al, V, Mn, Fe, Co, Rb, Cs, and U were consistently below 10, indicating a predominantly crustal (geogenic) origin for these elements (Wedepohl, 1995; Gabrieli et al., 2011). In contrast, Ni, and Sr displayed EFs greater than 10, suggesting contributions from mixed

sources. Notably, Ni exhibited exceptionally high EF values – above 100 – during autumn 2019 and spring 2020 (Ni). Mixed sources were also recognised for Li, K, Cr, Cu, Zn, As, Ag, Cd, and Tl with occasional EF values over 100. This suggests significant anthropogenic contributions, especially for Cu (spring and autumn 2019; spring 2020), As (from autumn 2020 to spring 2021), Zn (autumn 2019) and Cd (from autumn 2018 to spring 2019; winter 2019-20).

The 2019 springtime Pb concentration maxima are typically consistent with a mixture of eastern and western European sources (Sherrell et al., 2000; Bazzano et al., 2015, 2021). In this study, cluster mean trajectories obtained for winter 2018-2019 highlighted a 25% of air mass provenance from Russian Arctic and a 13% from eastern Siberia (Fig. S6), possibly explaining the higher concentrations of Pb revealed in spring 2019, following a reduced precipitation regime that occurred in January 2019. A local anthropogenic origin can be excluded though, since no activities (ordinary-extraordinary maintenance or particular events) were recorded in the vicinity of the sampling site in the 2019 sampling season. In addition, both GSRS and Ny-Ålesund (Fig. 1), located at 1 km of distance from each other, recorded comparable high concentrations of Pb, thus ruling out a possible contamination. However, at present, the long-range transport of Pb remains a hypothesis, likely supported by the breakdown of the wintry polar vortex (Fig. 2).

Backward trajectories (Fig. S6) for Ny-Ålesund area (78.92° N, 11.89° E) appear mostly in line with literature findings (Platt et al., 2022; Vecchiato et al., 2024), showing three main seasonal characters: a prevalent mass movement from ice-covered Central Arctic Ocean, Kara Sea, and Greenland Sea during autumn, a main provenance from Central Arctic Ocean and Kara Sea during winter, and a predominant trajectory from Northern Canada in addition to air masses arriving from Arctic Ocean and Kara seas during spring.

4.2 The main ion sources in the seasonal snow of Ny-Ålesund

Examining the dominant ions associated with marine aerosol, we found Cl⁻/Na⁺ median ratios ranging from 1.3 to 1.5 w w⁻¹, slightly lower than the expected value of 1.8 w w⁻¹ in the pure seawater (Zhuang et al., 1999), pointing the occurrence of a minimum Cl⁻ depletion in aerosol, quantified as 14% for the 2018-19 and 2019-20 campaigns, and as just 2% for the 2020-21 campaign. A possible explanation for this phenomenon could be the de-chlorination of sea-spray aerosol during transport. This reaction occurs when sea-salt particles containing NaCl interact with acids such as HNO₃, H₂SO₄, or organic acids, leading to the release of gaseous HCl (Zhuang et al., 1999, and reference therein). Although less likely, this process could also occur at the snow-atmosphere interface. On the

contrary, a possible influence of biomass burning on Cl⁻ depletion process has been excluded by the very low correlation (0.18, p value < 0.05) found between Cl⁻ depletion values and nss-K⁺/K⁺ ratios, which is a tracer of relative contribution of biomass burning (Song et al., 2018).

489

490

491

492

493

494

495

496

497

498

499

500

501

502

503

504

505

506

507

508

509

510

511

512

513

514

515

516

517

Positive correlations between Mg, Ca, and K⁺ with Na⁺ and Cl⁻ (Fig. 5, p value <0.05) suggest a common sea-spray source. However, the concentrations of Mg are also positively correlated with nss-Ca ($\rho_{load} = 0.55$), calculated according to Morales et al. (1998), indicating a shared non-marine source. This suggests that in addition to their marine origin, these ions (Mg, Ca) also have contributions from a non-marine, crustal source. Further evidence comes from the Ca/Mg ratios in surface snow samples collected during the three campaigns, which were higher than those found in seawater (0.32, Millero et al., 2008). This excess indicates the likely presence of mineral particles (i.e., calcite and dolomite), potentially originating from local rock or soil dust (e.g., limestone, dolostone, and marble, which are abundant in Svalbard), as previously observed by Barbaro et al. (2021). To further explore the mixed sources of these elements, we calculated the Enrichment Factors (EFs) of Mg and Ca. For Mg, the EF values were consistently above 10 in all the seasons analysed, indicating a significant non-crustal source (e.g., marine). In contrast, Ca displayed EF values greater than 10 only during autumn 2019, suggesting that its non-crustal contribution (likely from sea spray) was more pronounced during that specific season. Based on these findings, we conclude that Mg and Ca effectively share a common sea spray origin, but the sea-salt contribution of Ca was mainly significant in autumn 2019, while the excess of Ca in other seasons likely reflects inputs from crustal source, such as local mineral dust.

Similarly, sulphate (SO_4^{2-}) is highly and significantly correlated (p < 0.05) with both Na⁺ (ρ_{load} = 0.80) and Cl⁻ (ρ_{load} = 0.91), indicating that sea-spray is its main source. Nonetheless, Na⁺/SO₄²⁻ and Cl⁻/SO₄²⁻ ratios are significantly lower than typical seawater values (3.97 and 7.13, respectively, according to Millero et al., 2008) for the former two campaigns (2018-19, 2019-20). The elevated sulphate concentrations compared to sodium, also in winter snow, suggest the absence of a strong frost flower signature. Additionally, the lack of significant depletion in nss-SO₄²⁻ further supports the minimal role of frost flowers in contributing to the snow composition. Therefore, while frost flowers are known to impact snow chemistry in Svalbard (Rankin et al., 2002; Beaudon and Moore, 2009; Roscoe et al., 2011), our analysis indicates that their contribution to the observed sea salt peaks in Kongsfjorden during the 2018-19, 2019-20 campaigns was likely limited. This analysis highlights that, while sea ice extent supports higher sea-salt concentrations in snow, the specific sulphate and ion ratios observed point to sea spray as the main source, with only a minor role for frost flower-related inputs.

Instead, the presence of nss-SO₄²⁻ suggests potential inputs from other sources, such as crustal

material, anthropogenic emissions (e.g., fossil fuel combustion), or the oxidation of dimethylsulfide

520 (DMS) released from marine biological activities.

To estimate the crustal fraction of sulphate (cr-SO₄²⁻), the nss-Ca (as crustal marker) content was

multiplied by 0.59 (SO₄²-/Ca w/w ratio in the uppermost Earth crust - Wagenbach et al. 1996),

obtaining variable contributions for the three sampling campaigns, ranging from 2.45% up to 12.94%.

Conversely, the anthropogenic contribution to nss-SO₄²⁻ concentrations was investigated by the

application of the [ex- SO₄²⁻] concentration formula (Schwikowski et al., 1999), considering the

average concentration of [Ca] instead of the average ionic concentration [Ca²⁺] because Ca²⁺

concentrations were not measured in the samples collected during the second campaign due to

instrumental limitations:

519

522

523

524

525

526

527

528

529

531

532

533

534

535

536

537

538

539

540

541

542

543

544

$$[ex-SO_4^{2-}] = [SO_4^{2-}] - (0.12 [Na^+]) - (0.175 [Ca^{2+}])$$

The obtained results showed a 50 up to 60% of anthropogenic contribution for the nss-SO₄²⁻ input.

This finding corroborates previous results from Amore et al. (2022), who noted that anthropogenic

sulphate was the most abundant apportioned component at Gruvebadet, accounting for at least 50%

all over the year during the 2010-2019 investigated period. The plausible source of the anthropogenic

fraction is the atmospheric transport of secondary aerosols containing SO₄²-, and ammonium sulphate.

This sulphate can be formed by SO_x emitted from coal combustion throughout the winter and biomass

burning in the spring (Barbaro et al., 2021 and reference therein). The nss-SO₄²⁻ does not correlate

significantly with other ionic species (except for Mg), thus suggesting a separate origin (Fig. 5).

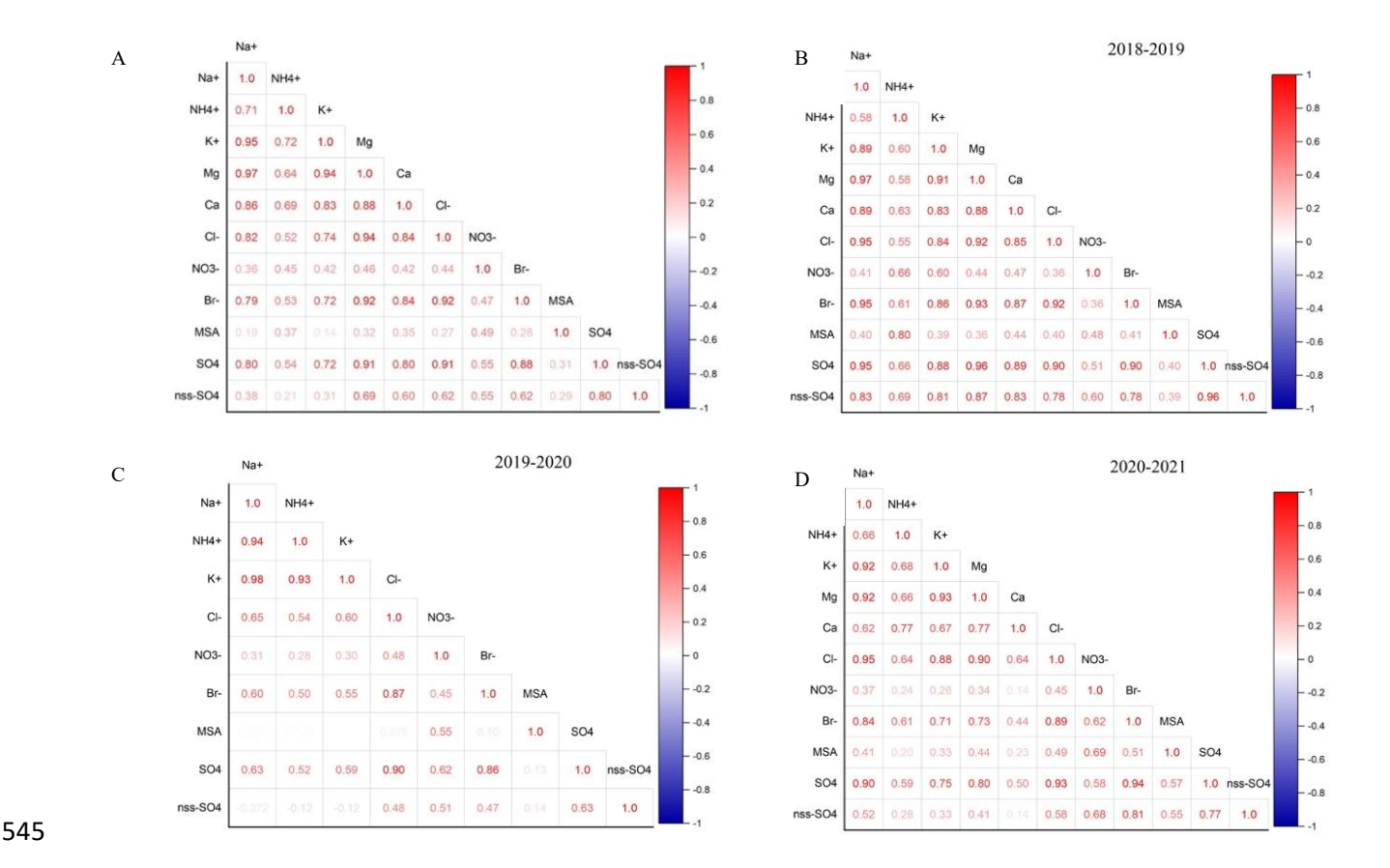


Fig. 5. Spearman correlation plots. A) Correlation plot for the three sampling seasons; B) Correlation plot for the 2018-2019 season; C) Correlation plot for the 2019-2020 season; D) Correlation plot for the 2020-2021 season.

To quantify the biogenic nss-SO₄²⁻ contribution, the methanesulfonic acid (MSA) loads - the final product of DMS oxidation - were multiplied by 3.0 (Udisti et al., 2016), revealing biogenic SO₄²⁻ contributions ranging from 0.15% (2018-19, 2020-21) up to 0.38% (2019-20). Furthermore, the MSA/nss-SO₄²⁻ ratio was inspected, revealing a mean value of 0.02 ± 0.03 during the first (2018-19) and the third (2020-21) sampling campaigns, and a maximum ratio equal to 0.06 ± 0.18 reached during the second campaign (2019-20), similar to the subarctic western North Pacific ratio found by Jung et al. (2014). However, several factors can influence MSA formation, a univocal marker of biogenic emissions, including higher biological productivity related to higher nutrient input; the concentrations of NO₃ radicals as key oxidants for DMS decomposition (higher NO₃ gives higher MSA); and lower air temperatures, which tend to yield higher MSA levels (Andreae et al., 1985; Udisti et al., 2020).

For the 2019-20 campaign, it seems likely that a combination of these three factors, together with the positive expansion of sea ice and the very close drift ice presence in March 2020, as revealed from satellite reconstructions (Fig. S7), contributed to the increased release of MSA in aerosol, and its consistent deposition in surface snow (Fig. 3). Indeed, DMS was likely accumulated under the sea

ice cover in the fjord and surrounding areas, and then being released and oxidised in the atmosphere when the ice broke off and melted (April-May). Furthermore, lower temperatures (-17.3°C in March 2020, compared to -16.1°C in March 2019, and -9.8°C in March 2021), positive correlation between MSA and NO₃⁻ (ρ_{load} = 0.49), and high-speed short-range transport (wind directions between 0°-60° and speeds > 5 m sec⁻¹) from the source to the near-coast sink site (GSRS) would have aided elevated concentrations of MSA in atmospheric depositions. However, the dominant south and southwest winds (180°-240°) during the major MSA peak in April 2020 (Fig. 3) likely transported marine aerosols and DMS from open ocean regions, further facilitating the increased MSA concentrations observed.

- Contrarily, in the 2018-19 season, sea ice lasted only until April and was restricted to the inner, shallower parts of Kongsfjorden (Assmy et al., 2023), possibly not allowing enough time with adequate sunlight for substantial biological activity to accumulate beneath or within it. This occurred despite the dominance in 2019, unlike the following year, of *Phaeocystis pouchetii*, a phytoplankton species known for its capacity to generate DMS in significant quantities, according to Assmy et al. (2023).
- Finally, the ammonium (NH₄⁺) load showed positive correlations (Fig. 5) with Na⁺ ($\rho_{load} = 0.71$), Cl⁻ ($\rho_{load} = 0.52$) and K⁺ ($\rho_{load} = 0.72$), as well as with SO₄²⁻ ($\rho_{load} = 0.54$), NO₃⁻ ($\rho_{load} = 0.45$), MSA ($\rho_{load} = 0.37$) and Br⁻ ($\rho_{load} = 0.53$), suggesting a close link with sea-salt ions and biogenic emissions. However, some contribution from biomass burning events and potential influence from anthropogenic activities cannot be excluded.

4.3 Bromine enrichment

The bromine enrichment factor (Br_{enr}) is well known to reflect specific processes (i.e., sea ice gas phase Br emission) that affect the Br concentration and load in the snowpack (Spolaor et al., 2014). Therefore, calculating the relative enrichment over the Br/Na ratio in sea water can offer crucial insights on sea ice variability for the investigated Arctic areas (Barbaro et al., 2021). As reported in previous studies (Maffezzoli et al., 2017; Barbaro et al., 2021), the Br enrichment factor (Br_{enr}) can be calculated as Br_{enr} = Br⁻ / (0.0065 Na⁺), where 0.0065 represents the Br⁻/Na⁺ seawater mass ratio. Contrarily to what observed in a former study (Barbaro et al., 2021) for the Hornsund area and northwestern Spitsbergen, where the Br_{enr} mean values were often < 1, indicating some Br⁻ depletion, in this study we observed Br_{enr} mean values ranging from 1.5 up to 17.7, with the highest value associated to the second sampling campaign conducted in 2019-20, which showed the most extensive

sea ice coverage. These results support the impact of the sea ice expansion and the close drift ice in the Kongsfjorden on the snow chemical composition. Indeed, newly formed sea ice releases gasphase Br into the polar atmosphere, thus supplying an extra Br⁻ source in addition to sea spray (Spolaor et al., 2016).

4.4 Anthropogenic and natural sources of ions and particulate trace elements

594

595

596

597

598

599

600

601

602

603

604

605

606

607

608

609

610

611

612

613

614

615

616

617

618

619

620

621

622

To complement the EFs analysis and further distinguish possible anthropogenic contributions from natural ones (marine and geogenic) for ions and particulate trace elements, a Hierarchical Cluster Analysis (HCA) method was carried out. Results of clustering (Fig. 6) clearly disentangle marine (Na⁺, Cl⁻, K⁺, NH₄⁺, SO₄²⁻, NO₃⁻, Br⁻, Mg, Sr, bio-SO₄²⁻, MSA), anthropogenic (As, Co, Ag, Ba, Cd, Zn, Pb, Bi, Cr, Cu, Ni), and geogenic (nss-Ca, Tl, Li, Al, Cs, Rb, Fe, Mn, U, Be, Se, V) sources of ionic and elemental species, considering the whole sampling campaign period (2018-2021). Interestingly, nss-SO₄²⁻ is brought together with the marine cluster, suggesting that its presence is largely influenced by marine biogenic sources, alongside contributions from secondary sulphate formation in the atmosphere. This indicates that nss-SO₄², despite having a variety of sources such as human contribution or dust, is closely linked to the marine environment. One important reason for this is the emission of DMS by phytoplankton. Additionally, secondary sulphate formation may have further contributed to the nss-SO₄²⁻. Co was grouped within the anthropogenic cluster in HCA, in contrast with EFs that suggested a crustal origin. This apparent discrepancy may reflect the relatively larger uncertainties typically associated with EF calculations, which can inherit errors from the choice of reference element, assumptions about crustal composition, and variability in background concentrations, compared to the more integrative approach of HCA (e.g., Reimann and de Caritat, 2000). Moreover, the trend for cobalt closely aligns with anthropogenic ones (e.g., As), while distinct trends are evident for crustal elements. Therefore, while the HCA results offer a reliable perspective on source differentiation and clustering patterns, they are best interpreted as complementary to the EF calculations rather than directly integrated with them. Incorporating EFs directly into the HCA could introduce significant inaccuracies, as EFs rely on reference element ratios that may vary and thus add complexity to the clustering process, potentially skewing the results. Consequently, HCA independently provides robust insights in this context, enhancing our understanding without the additional uncertainties that EF-based clustering might introduce.

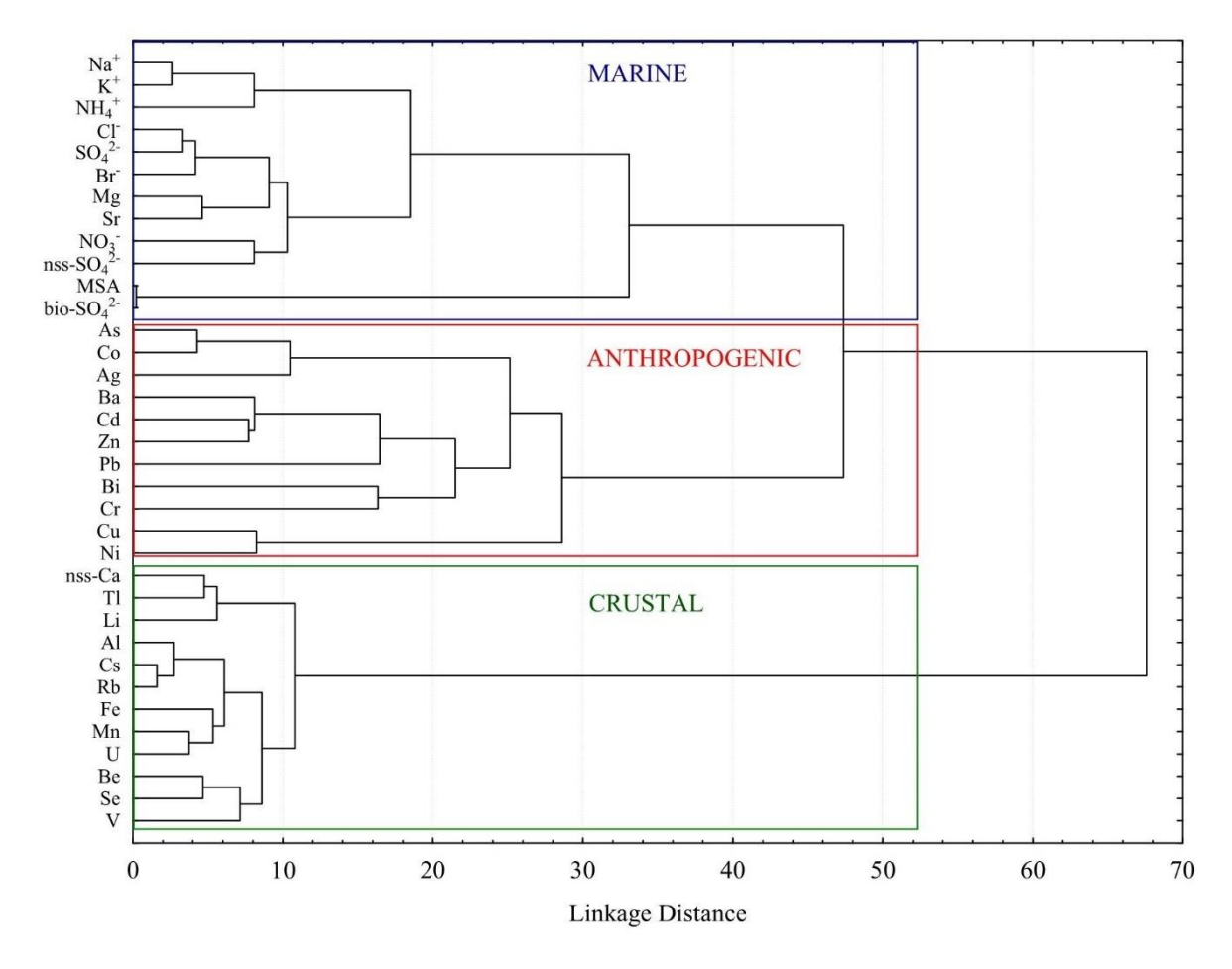


Fig. 6. Hierarchical cluster analysis applied to further disentangle the particulate trace element non-crustal sources.

5. Summary and Conclusion

In this study, trace elements and major ions were investigated in surface snow samples collected in Ny-Ålesund between October 2018 to June 2021. Seasonal and interannual variations of impurities have been observed, with general higher concentrations of marine species revealed in late spring 2020, associated to more extensive sea ice in Kongsfjorden in March 2020, promoted by negative temperature anomalies in both atmosphere and ocean and likely related to higher air mass recycle within the Arctic. These results provide direct evidence of how sea ice extent modulates the storage, release, and transport of marine-derived impurities, thereby influencing snow-atmosphere chemical exchange processes under varying climatic conditions. Higher concentrations in spring 2020 for geogenic and anthropogenic species are consistent with the influence of higher wind speeds, low atmospheric temperature anomalies, and generally drier conditions resulting from the exceptional occurrence of a strong and cold stratospheric polar vortex, accompanied by an unprecedently positive phase of the Arctic Oscillation in the troposphere during January-March 2020. While correlations between meteorological variables and concentrations were generally weak, the overall meteorological

context suggests that these unusual conditions likely contributed to the observed patterns. Such findings illustrate how large-scale atmospheric circulation anomalies associated with Arctic Amplification may significantly alter the deposition patterns of both natural and anthropogenic species in the snowpack. This is particularly evident especially in cold years, when the production of sea spray related aerosol likely derives by a larger extension of sea ice and stronger local Arctic circulation. The identification of geogenic, marine, and anthropogenic sources in the snowpack was allowed by a chemometric approach (HCA), which clarified the EFs results. The use of chemometric techniques (HCA) and back-trajectory analysis enabled a clearer attribution of sources and transport pathways, improving the interpretation of snow composition in relation to meteorological drivers. Specifically, the distinct seasonal air mass patterns revealed, characterised by dominant Arctic-origin air masses in fall and winter and a lack of expected mid-latitude inputs in spring, underscore the changing dynamics of snow-atmosphere interactions in a warming Arctic. Overall, these insights advance our understanding of how recent climatic anomalies, such as altered sea ice extent, shifts in Arctic Oscillation phases, and stronger polar vortices, modulate the chemical composition of the snowpack in Svalbard. Our findings highlight the sensitivity of snow-atmosphere exchanges to both local and large-scale climatic processes, offering important context for interpreting snow chemistry trends in a rapidly changing Arctic environment. Further statistical investigations, including multivariate and longer-term analyses, would be valuable for better quantifying these correlations.

Data availability

640

641

642

643

644

645

646

647

648

649

650

651

652

653

654

655

656

657

658

662

- The data supporting the findings of this study are available within the article and its supplementary materials. Other data that support the findings of this study are available from the corresponding
- author upon request.

Author contribution

AS: Conceptualization, Data curation, Investigation, Writing-original draft, Writing-review and 663 editing. EB: Conceptualization, Field work, Data curation, Formal Analysis, Writing-original draft, 664 Writing-review and editing, Funding acquisition. MF: Formal Analysis, Field work, Data curation, 665 Writing-review and editing. FS: Field work, Formal analysis, Investigation, Writing-review and 666 editing. MV: Writing-review and editing. MV: Field work, Writing-review and editing. MM: 667 Investigation. FB: Investigation, Writing-review and editing. FB: Investigation. Field work. CJMH: 668 669 Investigation, Data curation, Writing-review and editing. AB: Field work, Data curation, Writingreview and editing. AG: Resources, Supervision, Validation, Writing-review and editing, Funding 670

- 671 acquisition. CB: Resources, Supervision, Validation, Writing-review and editing, Funding
- acquisition. AS: Funding acquisition, Supervision, Validation, Writing-review and editing.

Competing interests

673

675

The authors declare that they have no conflict of interest.

Acknowledgments

- This project has received funding from the European Union's Horizon 2020 research and innovation
- programme under grant agreement no. 689443 via ERA PLANET Strand 4 project iCUPE
- 678 (Integrative and Comprehensive Understanding on Polar Environments). We are grateful to the Arctic
- 679 Station Dirigibile Italia from the Italian National Research Council Institute of Polar Science (CNR-
- 680 ISP) for logistical support. The authors gratefully acknowledge Claudio Artoni, Maria Papale, Ivan
- 681 Sartorato, Federico Dallo, Alice Callegaro, Marco Casula, Mariasilvia Giamberini, Fabio Giardi, and
- all the station leaders of "Dirigibile Italia" who participated and offered valuable help and logistic
- support during the 2018-2021 sampling campaigns. Furthermore, we acknowledge Klara Wolf, Linda
- Rehder, and Ane Kvernvik for help with CTD sampling. We acknowledge the help of ELGA
- LabWater in providing the PURELAB Pulse and PURELAB Flex, which produced the ultrapure
- water used in these experiments.

References

687

- Amore, A., Giardi, F., Becagli, S., Caiazzo, L., Mazzola, M., Severi, M., Traversi, R.: Source apportionment of sulphate in the High Arctic by a 10 yr-long record from Gruvebadet Observatory (Ny-Ålesund, Svalbard Islands). Atmos. Environ., 270, 118890, 1-10,
- 691 https://doi.org/10.1016/j.atmosenv.2021.118890, 2022
- Andreae, M.O., Ferek, R.J., Bermond, F., Byrd, K.P., Engstrom, R.T., Hardin, S., Houmere,
- P.D., LeMarrec, F., Raemdonck, H., Chatfield, R.B.: Dimethyl sulfide in the marine atmosphere,
- J. Geophys. Res., 90, D7, 12891-12900, https://doi.org/10.1029/JD090iD07p12891, 1985
- Assmy, P., Kvernvik, A.C., Hop, H., Hoppe, C.J.M., Chierici, M., David, D., Duarte, P.,
- 697 Fransson, A., Garcia, L.M., Patuła, W., Kwaśniewski, S., Maturilli, M., Pavlova, O., Tatarek, A.,
- 698 Wiktor, J.M., Wold, A., Wolf, K.K.E., Bailey, A.: Seasonal plankton dynamics in Kongsfjorden
- 699 during two years of contrasting environmental conditions, Prog. Oceanogr., 213, 102996,
- 700 https://doi.org/10.1016/j.pocean.2023.102996, 2023
- Barbaro, E., Koziol, K., Björkman, M.P., Vega, C.P., Zdanowicz, C., Martma, T., Gallet, J.C.,
- Kępski, D., Larose, C., Luks, B., Tolle, F., Schuler, T. V., Uszczyk, A., Spolaor, A.: Measurement
- report: Spatial variations in ionic chemistry and water-stable isotopes in the snowpack on glaciers
- across Svalbard during the 2015-2016 snow accumulation season, Atmos. Chem. Phys., 21, 3163–
- 705 3180, https://doi.org/10.5194/acp-21-3163-2021, 2021

- Barbaro, E., Padoan, S., Kirchgeorg, T., Zangrando, R., Toscano, G., Barbante, C., Gambaro,
- 707 A.: Particle size distribution of inorganic and organic ions in coastal and inland Antarctic aerosol,
- 708 Environ. Sci. Pollut. Res., 24, 2724-2733, https://doi.org/10.1007/s11356-016-8042-x, 2017
- Barbaro, E., Zangrando, R., Vecchiato, M., Piazza, R., Cairns, W.R.L., Capodaglio, G.,
- 710 Barbante, C., Gambaro, A.: Free amino acids in Antarctic aerosol: Potential markers for the evolution
- and fate of marine aerosol, Atmos. Chem. Phys., 15, 5457–5469, https://doi.org/10.5194/acp-15-
- 712 5457-2015, 2015
- Bazzano, A., Ardini, F., Becagli, S., Traversi, R., Udisti, R., Cappelletti, D., Grotti, M.: Source
- assessment of atmospheric lead measured at Ny-Ålesund, Svalbard, Atmos. Environ., 113, 20-26,
- 715 https://doi.org/10.1016/j.atmosenv.2015.04.053, 2015
- Bazzano, A., Bertinetti, S., Ardini, F., Cappelletti, D., Grotti, M.: Potential Source Areas for
- 717 atmospheric Lead reaching Ny-Ålesund from 2010 to 2018, Atmos., 12, 388, 1-17,
- 718 https://doi.org/10.3390/atmos12030388, 2021
- Beaudon, E., Moore, J.: Frost flower chemical signature in winter snow on Vestfonna ice cap,
- 720 Nordaustlandet, Svalbard, Cryosphere, 3, 147–154, https://doi.org/10.5194/tc-3-147-2009, 2009
- Beine, H.J., Dominé, F., Ianniello, A., Nardino, M., Allegrini, I., Teinilä, K., Hillamo, R.:
- 722 Fluxes of nitrates between snow surfaces and the atmosphere in the European high Arctic, Atmos.
- 723 Chem. Phys., 3, 335-346, https://doi.org/10.5194/acp-3-335-2003, 2003
- Bertò, M., Cappelletti, D., Barbaro, E., Varin, C., Gallet, J.-C., Markowicz, K.,
- 725 Rozwadowska, A., Mazzola, M., Crocchianti, S., Poto, L., Laj, P., Barbante, C., Spolaor, A.:
- Variability in black carbon mass concentration in surface snow at Svalbard, Atmos. Chem. Phys., 21,
- 727 12479-12493, https://doi.org/10.5194/acp-21-12479-2021, 2021
- Björkman, M., Kühnel, R., Partridge, D.G., Roberts, T.J., Aas, W., Mazzola, M., Viola, A.,
- 729 Hodson, A., Ström, J., Isaksson, E.: Nitrate dry deposition in Svalbard, Tellus B, 65(1),
- 730 https://doi.org/10.3402/tellusb.v65i0.19071, 2013
- Chylek, P., Folland, C., Klett, J.D., Wang, M., Hengartner, N., Lesins, G., Dubey, M.K.:
- Annual Mean Arctic Amplification 1970-2020. Observed and Simulated by CMIP6 Climate Models,
- 733 Geophys. Res. Lett., 49 (13), e2022GL099371, https://doi.org/10.1029/2022GL099371, 2022
- D'Amico, M., Kallenborn, R., Scoto, F., Gambaro, A., Gallet, J.-C., Spolaor, A., Vecchiato,
- 735 M.: Chemicals of Emerging Arctic Concern in north-western Spitsbergen snow: Distribution and
- 736 sources, Sci. Total Environ., 908, 168401, https://doi.org/10.1016/j.scitotenv.2023.168401, 2024
- Dethloff, K., Maslowski, W., Hendricks, S., Lee, Y.J., Goessling, H.F., Krumpen, T., Haas,
- 738 C., Handorf, D., Ricker, R., Bessnov, V., Cassano, J.J., Kinney, J.C., Osinski, R., Rex, M., Rinke, A.,
- 739 Sokolova, J., Sommerfeld, A.: Arctic sea ice anomalies during the MOSAiC winter 2019/20,
- 740 Cryosphere, 16, 981-1005, https://doi.org/10.5194/tc-16-981-2022, 2022
- Draxler, R.R.: An overview of the HYSPLIT 4 modelling system for trajectories, dispersion
- and deposition, Aust. Meteorol. Mag., 47, 295–308, 1998
- Dunn, O.J.: Multiple comparisons among means, J. Am. Stat. Assoc., 56, 293,
- 744 https://doi.org/10.1080/01621459.1961.10482090, 1961

- Eleftheriadis, K., Vratolis, S., Nyeki, S.: Aerosol black carbon in the European Arctic:
- Measurements at Zeppelin station, Ny-Ålesund, Svalbard from 1998-2007, Geophys. Res. Lett., 36,
- 747 1–5, https://doi.org/10.1029/2008GL035741, 2009
- Feltracco, M., Barbaro, E., Hoppe, C.J.M., Wolf, K.K.E., Spolaor, A., Layton, R., Keuschnig,
- 749 C., Barbante, C., Gambaro, A., Larose, C.: Airborne bacteria and particulate chemistry capture
- 750 Phytoplankton bloom dynamics in an Arctic fjord, Atmos. Environ., 256, 118458,
- 751 https://doi.org/10.1016/j.atmosenv.2021.118458, 2021
- Feltracco, M., Barbaro, E., Tedeschi, S., Spolaor, A., Turetta, C., Vecchiato, M., Morabito,
- 753 E., Zangrando, R., Barbante, C., Gambaro, A.: Interannual variability of sugars in Arctic aerosol:
- 754 Biomass burning and biogenic inputs, Sci. Total Environ., 706, 136089,
- 755 https://doi.org/10.1016/j.scitotenv.2019.136089, 2020
- Geng, H., Ryu, J., Jung, H.J., Chung, H., Ahn, K.H.O., Ro, C.U.N.: Single-particle
- characterization of summertime arctic aerosols collected at Ny-Ålesund, Svalbard, Environ. Sci.
- 758 Technol., 44, 2348–2353, https://doi.org/10.1021/es903268j, 2010
- George, B.J., Gains-Germain, L., Broms, K., Black, K., Furman, M., Hays, M.D., Thomas,
- 760 K.W., Simmons, J.E.: Censoring trace-level environmental data: statistical analysis considerations to
- 761 limit bias, Environ. Sci. Technol., 55(6), 3786-3795, https://doi.org/10.1021/acs.est.0c02256, 2021
- Gerland, S., Pavlova, O., Marnela, M., Divine, D.V., Kohler, J., Renner, A., Skoglund, A.:
- Sea ice extent variability in Kongsfjorden, Svalbard during 2003-2021, based on visual observations
- 764 from the mountain Zeppelinfiellet, Norwegian Polar Institute,
- 765 https://doi.org/10.21334/npolar.2022.d6d31f5b, 2022
- Gjermundsen, A., Seland Graff, L., Bentsen, M., Anders Breivik, L., Boldingh Debernard, J.,
- Makkonen, R., Olivié, D.J.L., Seland, Ø., Zieger, P., Schulz, M.: How representative is Svalbard for
- future Arctic climate evolution? An Earth system modelling perspective (SvalCLIM), SESS Report
- 769 2020 The State of Environmental Science in Svalbard, https://doi.org/10.5281/zenodo.4034104,
- 770 2020
- Hansen, B.B., Isaksen, K., Benestad, R.E., Kohler, J., Pedersen, Å., Loe, L.E., Coulson, S.J.,
- Larsen, J.O., Varpe, Ø.: Warmer and wetter winters: Characteristics and implications of an extreme
- 773 weather event in the High Arctic, Environ. Res. Lett., 9, https://doi.org/10.1088/1748-
- 774 9326/9/11/114021, 2014
- Hodgkins, R., Tranter, M.: Solute in High Arctic glacier snow cover and its impact on runoff
- 776 chemistry, Ann. Glaciol., 26, 156-160, https://doi.org/10.3189/1998AoG26-1-156-160, 1998
- Jacobi, H.-W., Obleitner, F., Da Costa, S., Ginot, P., Eleftheriadis, K., Aas, W., Zanatta, M.:
- 778 Deposition of ionic species and black carbon to the Arctic snowpack: combining snow pit
- observations with modeling, Atmos. Chem. Phys., 19, 10361-10377,
- 780 https://doi.org/10.3402/tellusb.v65i0.19071, 2019
- Jung, J., Furutani, H., Uematsu, M., Park, J.: Distributions of atmospheric non-sea-salt
- sulphate and methanesulfonic acid over the Pacific Ocean between 48°N and 55°S during summer,
- 783 Atmos. Environ., 99, 374-384, https://doi.org/10.1016/j.atmosenv.2014.10.009, 2014

- Koziol, K., Uszczyk, A., Pawlak, F., Frankowski, M., Polkowska, Ż.: Seasonal and Spatial Differences in Metal and Metalloid Concentrations in the Snow Cover of Hansbreen, Svalbard, Front.
- 786 Earth Sci., 8, 1–8, https://doi.org/10.3389/feart.2020.538762, 2021
- Lai, A.M., Shafer, M.M., Dibb, J.E., Polashenski, C.M., Schauer, J.J.: Elements and inorganic ions as source tracers in recent Greenland snow, Atmos. Environ., 164, 205–215, https://doi.org/10.1016/j.atmosenv.2017.05.048, 2017
- Lawrence, Z.D., Perlwitz, J., Butler, A.H., Manney, G.L., Newman, P.A., Lee, S.H., Nash, E.R.: The Remarkably Strong Arctic Stratospheric Polar Vortex of Winter 2020: Links to Record-Breaking Arctic Oscillation and Ozone Loss, J. Geophys. Res. Atmos., 125, 1–21, https://doi.org/10.1029/2020JD033271, 2020
- Maffezzoli, N., Spolaor, A., Barbante, C., Bertò, M., Frezzotti, M., Vallelonga, P.: Bromine, iodine and sodium in surface snow along the 2013 Talos Dome-GV7 traverse (northern Victoria Land, East Antarctica), Cryosphere, 11, 693-705, https://doi.org/10.5194/tc-11-693-2017, 2017
- Millero, F.J., Feistel, R., Wright, D.G., McDougall, T.J.: The composition of Standard Seawater and the definition of the Reference-Composition Salinity Scale, Deep-Sea Res., 55, 50–72, 2008
- Morales, J.A., Pirela, D., de Nava, M.G., de Borrego, B.S., Velásquez, H., Durán, J.: Inorganic water soluble ions in atmospheric particles over Maracaibo Lake Basin in the western region of Venezuela, Atmos. Res., 46, https://doi.org/10.1016/S0169-8095(97)00071-9, 1998
- Nawrot, A.P., Migała, K., Luks, B., Pakszys, P., Głowacki, P.: Chemistry of snow cover and acidic snowfall during a season with a high level of air pollution on the Hans Glacier, Spitsbergen, Polar Sci., 10, 249–261, https://doi.org/10.1016/j.polar.2016.06.003, 2016
- Platt, S.M., Hov, Ø., Berg, T., Breivik, K., Eckhardt, S., Eleftheriadis, K., Evangeliou, N.,
- Fiebig, M., Fisher, R., Hansen, G., Hansson, H.-C., Heintzenberg, J., Hermansen, O., Heslin-Rees,
- 808 D., Holmén, K., Hudson, S., Kallenborn, R., Krejci, R., Krognes, T., Larssen, S., Lowry, D., Lund
- Myhre, C., Lunder, C., Nisbet, E., Nizzetto, P.B., Park, K.-T., Pedersen, C.A., Pfaffhuber, K.A., Röckmann, T., Schmidbauer, N., Solberg, S., Stohl, A., Ström, J., Svendby, T., Tunved, P., Tørnkvist,
- Kockmann, I., Schindbauer, N., Soberg, S., Stolii, A., Strolli, J., Svendoy, I., Tunved, F., Tørnkvist, K., van der Veen, C., Vratolis, S., Yoon, Y.L., Yttri, K.E., Zieger, P., Aas, W., Tørseth, K.:
- 812 Atmospheric composition in the European Arctic and 30 years of the Zeppelin Observatory, Ny-
- 813 Ålesund, Atmos. Chem. Phys., 22, 3321-3369, https://doi.org/10.5194/acp-22-3321-2022, 2022
- Pomeroy, J.W.: A process-based model of snow drifting, Ann. Glaciol., 13, 237-240, https://doi.org/10.3189/S0260305500007965, 1989
- Rankin, A.M., Wolff, E.W.: Frost flowers: Implications for tropospheric chemistry and ice core interpretation, J. Geophys. Res., 107, D23, 4683, https://doi.org/10.1029/2002JD002492, 2002
- Rantanen, M., Karpechko, A.Y., Lipponen, A., Nordling, K., Hyvärinen, O., Ruosteenoja, K., Vihma, T., Laaksonen, A.: The Arctic has warmed nearly four times faster than the globe since 1979, Commun. Earth Environ, 3, 168, https://doi.org/10.1038/s43247-022-00498-3, 2022
- Reimann, C., De Caritat, P.: Intrinsic flaws of element Enrichment Factors (EFs) in environmental geochemistry, Environ. Sci. Technol., 34, https://doi.org/10.1021/es0013390, 2000

- Rinke, A., Maturilli, M., Graham, R.M., Matthes, H., Handorf, D., Cohen, L., Hudson, S.R.,
- Moore, J.C.: Extreme cyclone events in the Arctic: Wintertime variability and trends, Environ. Res.
- 825 Lett., 12, https://doi.org/10.1088/1748-9326/aa7def, 2017
- Roscoe, H.K., Brooks, B., Jackson, A.V., Smith, M.H., Walker, S.J., Obbard, R.W., Wolff,
- 827 E.W.: Frost flowers in the laboratory: Growth, characteristics, aerosol, and the underlying sea ice, J.
- 828 Geophys. Res., 116, D12301, https://doi.org/10.1029/2010JD015144, 2011
- Ruppel, M.M., Khedr, M., Liu, X., Beaudon, E., Szidat, S., Tunved, P., Ström, J., Koponen,
- H., Sippula, O., Isaksson, E., Gallet, J.-C., Hermanson, M., Manninen, S., Schnelle-Kreis, J.: Organic
- compounds, radiocarbon, trace elements and atmospheric transport illuminating sources of elemental
- 832 carbon in a 300-year Svalbard ice core, J. Geophys. Res.: Atmos., 128,
- 833 https://doi.org/10.1029/2022JD038378, 2023
- Salzano, R., Cerrato, R., Scoto, F., Spolaor, A., Valentini, E., Salvadore, M., Esposito, G.,
- 835 Sapio, S., Taramelli, A., Salvatori, R.: Detection of winter heat wave impact on surface runoff in a
- 836 periglacial environment (Ny-Ålesund, Svalbard), Remote Sens., 15(18), 4435,
- 837 https://doi.org/10.3390/rs15184435, 2023
- Schoeberl, M.R., Newman, P.A.: Middle Atmosphere: Polar Vortex, Encyclopedia of
- Atmospheric Sciences, Second Edition, Elsevier, 12-17, https://doi.org/10.1016/B978-0-12-382225-
- 840 3.00228-0, 2015
- Schwikowski, M., Döscher, A., Gäggeler, H.W., Schotterer, U.: Anthropogenic versus natural
- sources of atmospheric sulphate from an Alpine ice core. Tellus B: Chemical and Physical
- 843 Meteorology, 51:5, 938-951, https://doi.org/10.3402/tellusb.v51i5.16506, 1999
- Scoto, F., Pappaccogli, G., Mazzola, M., Donateo, A., Salzano, R., Monzali, M., de Blasi, F.,
- Larose, C., Gallet, J.-C., Decesari, S., Spolaor, A.: Automated observation of physical snowpack
- 846 properties in Ny-Ålesund, Front. Earth Sci., 11:1123981, 1-9, https://doi.org/
- 847 0.3389/feart.2023.1123981, 2023
- Serreze, M.C., Barry, R.G.: Processes and impacts of Arctic amplification: A research
- synthesis, Glob. Planet. Change, 77, 85-96, http://dx.doi.org/10.1016/j.gloplacha.2011.03.004, 2011
- Sherrell, R.M., Boyle, E.A., Harris, N.R., Falkner, K.K.: Temporal variability of Cd, Pb, and
- 851 Pb isotope deposition in central Greenland snow, Geochem Geophys, 1 (1), 1-22,
- https://doi.org/10.1029/1999GC000007, 2000
- Sobota, I., Weckwerth, P., Grajewski, T.: Rain-On-Snow (ROS) events and their relations to
- snowpack and ice layer changes on small glaciers in Svalbard, the high Arctic, J. Hydrol, 590, 125279,
- 855 https://doi.org/10.1016/j.jhydrol.2020.125279, 2020
- 856 Song, C., Becagli, S., Beddows, D.C.S., Brean, J., Browse, J., Dai, Q., Dall'Osto, M., Ferracci,
- 857 V., Harrison, R.M., Harris, N., Li, W., Jones, A.E., Kirchgäßner, A., Kramawijaya, A.G., Kurganskiy,
- 858 A., Lupi, A., Mazzola, M., Severi, M., Traversi, R., Shi, Z.: Understanding sources and drivers of
- size-resolved aerosol in the High Arctic islands of Svalbard using a receptor model coupled with
- machine learning, Environ. Sci. Technol., 56, 11189-11198, https://doi.org/10.1021/acs.est.1c07796,
- 861 2022
- Song, J., Zhao, Y., Zhang, Y., Fu, P., Zheng, L., Yuan, Q., Wang, S., Huang, X., Xu, W., Cao,
- 863 Z., Gromov, S., Lai, S.: Investigation of biomass burning on atmospheric aerosols over the western

- 864 South China Sea: Insights from ions, carbonaceous fractions and stable carbon isotope ratios,
- 865 Environ. Pollut., 242, 1800-1809, https://doi.org/10.1016/j.envpol.2018.07.088, 2018
- Spolaor, A., Scoto, F., Larose, C., Barbaro, E., Burgay, F., Bjorkman, M., Cappelletti, D.,
- Dallo, F., de Blasi, F., Divine, D., Dreossi, G., Gabrieli, J., Isaksson, E., Kohler, J., Martma, T.,
- 868 Schmidt, L.S., Schuler, T.V., Stenni, B., Turetta, C., Luks, B., Casado, M., Gallet, J.-C.: Climate
- shape is rapidly deteriorating the climatic signal in Svalbard glaciers, Cryosphere, 18, 307-320,
- 870 https://doi.org/10.5194/tc-18-307-2024, 2024
- 871 Spolaor, A., Varin, C., Pedeli, X., Christille, J.M., Kirchgeorg, T., Giardi, F., Cappelletti, D.,
- Turetta, C., Cairns, W.R.L., Gambaro, A., Bernagozzi, A., Gallet, J.C., Björkman, M.P., Barbaro, E.:
- 873 Source, timing and dynamics of ionic species mobility in the Svalbard annual snowpack, Sci. Total
- 874 Environ., 751, 141640, https://doi.org/10.1016/j.scitotenv.2020.141640, 2021b
- Spolaor, A., Moroni, B., Luks, B., Nawrot, A., Roman, M., Larose, C., Stachnik, Ł., Bruschi,
- 876 F., Kozioł, K., Pawlak, F., Turetta, C., Barbaro, E., Gallet, J.-C., Cappelletti, D.: Investigation on the
- 877 Sources and Impact of Trace Elements in the Annual Snowpack and the Firn in the Hansbreen
- 878 (Southwest Spitsbergen), Front. Earth Sci., 8, 1–10, https://doi.org/10.3389/feart.2020.536036, 2021a
- Spolaor, A., Barbaro, E., Cappelletti, D., Turetta, C., Mazzola, M., Giardi, F., Björkman, M.P.,
- 880 Lucchetta, F., Dallo, F., Aspmo Pfaffhuber, K., Angot, H., Dommergue, A., Maturilli, M., Saiz-
- 881 Lopez, A., Barbante, C., Cairns, W.R.L.: Diurnal cycle of iodine, bromine, and mercury
- 882 concentrations in Svalbard surface snow, Atmos. Chem. Phys., 19, 13325–13339,
- 883 https://doi.org/10.5194/acp-19-13325-2019, 2019
- Spolaor, A., Angot, H., Roman, M., Dommergue, A., Scarchilli, C., Vardè, M., Del Guasta,
- 885 M., Pedeli, X., Varin, C., Sprovieri, F., Magand, O., Legrand, M., Barbante, C., Cairns, W.R.L:
- 886 Feedback mechanisms between snow and atmospheric mercury: Results and observations from field
- 887 campaigns on the Antarctic plateau, Chemosphere, 197, 306–317,
- 888 https://doi.org/10.1016/j.chemosphere.2017.12.180, 2018
- Spolaor, A., Opel, T., McConnell, J.R., Maselli, O.J., Spreen, G., Varin, C., Kirchgeorg, T.,
- 890 Fritzsche, D., Saiz-Lopez, A., Vallelonga, P.: Halogen-based reconstruction of Russian Arctic sea ice
- 891 area from the Akedemii Nauk ice core (Severnaya Zemlya), Cryosphere, 10, 245-256,
- 892 https://doi.org/10.5194/tc-10-245-2016, 2016
- Spolaor, A., Vallelonga, P., Gabrieli, J., Martma, T., Björkman, M.P., Isaksson, E., Cozzi, G.,
- Turetta, C., Kjær, H.A., Curran, M.A.J., Moy, A.D., Schönhardt, A., Blechschmidt, A.-M., Burrows,
- J.P., Plane, J.M.C., Barbante, C.: Seasonality of halogen deposition in polar snow and ice, Atmos.
- 896 Chem. Phys., 14, 18, 9613-9622, https://doi.org/10.5194/acp-14-9613-2014, 2014
- Stein, A.F., Draxler, R.R., Rolph, G.D., Stunder, B.J.B., Cohen, M.D., Ngan, F.: Noaa's
- 898 hysplit atmospheric transport and dispersion modeling system, Bull. Am. Meteorol. Soc., 96, 2059-
- 899 2077, https://doi.org/10.1175/BAMS-D-14-00110.1, 2015
- Stohl, A., Berg, T., Burkhart, J.F., Fjæraa, a. M., Forster, C., Herber, A., Hov, Ø., Lunder, C.,
- 901 McMillan, W.W., Oltmans, S., Shiobara, M., Simpson, D., Solberg, S., Stebel, K., Ström, J., Tørseth,
- 902 K., Treffeisen, R., Virkkunen, K., Yttri, K.E.: Arctic smoke record high air pollution levels in the
- 903 European Arctic due to agricultural fires in Eastern Europe, Atmos. Chem. Phys. Discuss., 6, 9655–
- 904 9722, https://doi.org/10.5194/acpd-6-9655-2006, 2006b

- Stohl, A., Berg, T., Burkhart, J.F., Fjæraa, a. M., Forster, C., Herber, A., Hov, Ø., Lunder, C.,
- 906 McMillan, W.W., Oltmans, S., Shiobara, M., Simpson, D., Solberg, S., Stebel, K., Ström, J., Tørseth,
- 907 K., Treffeisen, R., Virkkunen, K., Yttri, K.E.: Arctic smoke record high air pollution levels in the
- 908 European Arctic due to agricultural fires in Eastern Europe, Atmos. Chem. Phys. Discuss., 6, 9655–
- 909 9722, https://doi.org/10.5194/acpd-6-9655-2006, 2006a
- Turetta, C., Feltracco, M., Barbaro, E., Spolaor, A., Barbante, C., Gambaro, A.: A year-round
- 911 measurement of water-soluble trace and rare earth elements in arctic aerosol: Possible inorganic
- tracers of specific events, Atmosphere, 12, https://doi.org/10.3390/atmos12060694, 2021
- 913 Udisti, R., Traversi, R., Becagli, S., Tomasi, C., Mazzola, M., Lupi, A., Quinn, P.K.: Arctic
- Aerosols, in: Physics and Chemistry of the Arctic Atmosphere, Springer Polar Sciences, edited by:
- 915 Kokhanovsky, A., Tomasi, C., 209-329, https://doi.org/10.1007/978-3-030-33566-3 4, 2020
- Udisti, R., Bazzano, A., Becagli, S., Bolzacchini, E., Caiazzo, L., Cappelletti, D., Ferrero, L.,
- 917 Frosini, D., Giardi, F., Grotti, M., Lupi, A., Malandrino, M., Mazzola, M., Moroni, B., Severi, M.,
- 918 Traversi, R., Viola, A., Vitale, V.: Sulphate source apportionment in the Ny-Ålesund (Svalbard
- 919 Islands) Arctic aerosol, Rend. Fis. Acc. Lincei, 27, Suppl 1: S85-S94, https://doi.org/10.1007/s12210-
- 920 016-0517-7, 2016
- Van Hecke, T.: Power study of anova versus Kruskal-Wallis test, J. Stat. Manag. Syst., 15, 2-
- 922 3, https://doi.org/10.1080/09720510.2012.10701623, 2013
- Vecchiato, M., Barbante, C., Barbaro, E., Burgay, F., Cairns, W.R.L., Callegaro, A.,
- 924 Cappelletti, D., Dallo, F., D'Amico, M., Feltracco, M., Gallet J.-C., Gambaro, A., Larose, C.,
- 925 Maffezzoli, N., Mazzola, M., Sartorato, I., Scoto, F., Turetta, C., Vardè, M., Xie, Z., Spolaor, A.: The
- 926 seasonal change of PAHs in Svalbard surface snow, Environ. Pollut., 340, 122864,
- 927 https://doi.org/10.1016/j.envpol.2023.122864, 2024
- Vecchiato, M., Barbaro, E., Spolaor, A., Burgay, F., Barbante, C., Piazza, R., Gambaro, A.:
- 929 Fragrances and PAHs in snow and seawater of Ny-Ålesund (Svalbard): Loca and long-range
- 930 contamination, Environ. Pollut., 242, 1740-1747, https://doi.org/10.1016/j.envpol.2018.07.095, 2018
- Vega, C.P., Björkman, M.P., Pohjola, V.A., Isaksson, E., Pettersson, R., Martma, T., Marca,
- A., Kaiser, J., Vega, C.P., Björkman, M.P., Pohjola, V.A., Isaksson, E., Pettersson, R., Martma, T.,
- 933 Marca, A., Kaiser, J., Pohjola, V.A., Isaksson, E., Pettersson, R., Vega, C.P., Bjo, M.P.: Nitrate stable
- 934 isotopes and major ions in snow and ice samples from four Svalbard sites Nitrate stable isotopes and
- major ions in snow and ice samples from four Svalbard sites, Polar Res., 2015, 34, 23246,
- 936 https://doi.org/10.3402/polar.v34.23246, 2015
- Wagenbach, D., Preunkert, S., Schäfer, J., Jung, W., Tomadin, L.: Northward transport of
- 938 Saharan dust recorded in a deep alpine ice core, in: The impact of desert dust across the
- mediterranean, Springer, The Netherlands, edited by: Guerzoni, S., Chester, R., 291-300, 1996
- Wedepohl, K.H.: The composition of the chemical crust. Geoch. Cosm. Act., 59(7), 1217-
- 941 1232, https://doi.org/10.1016/0016-7037(95)00038-2, 1995
- Yttri, K.E., Lund Myhre, C., Eckhardt, S., Fiebig, M., Dye, C., Hirdman, D., Ström, J.,
- 943 Klimont, Z., Stohl, A.: Quantifying black carbon from biomass burning by means of levoglucosan -
- A one-year time series at the Arctic observatory Zeppelin, Atmos. Chem. Phys., 14, 6427–6442,
- 945 https://doi.org/10.5194/acp-14-6427-2014, 2014a

Zhan, J., Gao, Y., Li, W., Chen, L., Lin, H., Lin, Q.: Effects of ship emissions on summertime 946 the Res., 500-510, aerosols at Ny-Alesund in Arctic, Atmos. Pollut. 5, 947 https://doi.org/10.5094/APR.2014.059, 2014 948 Zhuang, H., Chan, C.K., Fang, M., Wexler, A.S.: Size distributions of particulate sulphate, 949 nitrate, and ammonium at a coastal site in Hong Kong, Atmos. Environ., 33, 843-853, 1999 950 951 952